NASA CR-72855
R-8406

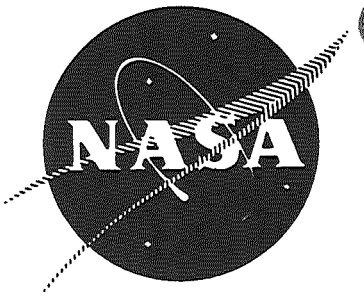

PROTECTIVE COATING SYSTEM FOR A REGENERATIVELY COOLED THRUST CHAMBER

FINAL REPORT

(1 February 1969 Through 31 December 1970)

by

H. W. Carpenter

prepared for

NATIONAL AERONAUTICS AND SPACE ADMINISTRATION

Contract NAS3-11187

ROCKETDYNE

A Division of North American Rockwell Corporation
Canoga Park, California

NOTICE

This report was prepared as an account of Government-sponsored work. Neither the United States, nor the National Aeronautics and Space Administration (NASA), nor any person acting on behalf of NASA:

1. Makes any warranty or representation, expressed or implied, with respect to the accuracy, completeness, or usefulness of the information contained in this report, or that the use of any information, apparatus, method, or process disclosed in this report may not infringe privately-owned rights; or

2. Assumes any liabilities with respect to the use of, or for damages resulting from the use of, any information, apparatus, method or process disclosed in this report.

As used above, "person acting on behalf of NASA" included any employee or contractor of NASA, or employee of such contractor, to the extent that such employee or contractor of NASA or employee of such contractor prepares, disseminates, or provides access to any information pursuant to his employment or contract with NASA, or his employment with such contractor.

Requests for copies of this report should be referred to:

National Aeronautics and Space Administration
Scientific and Technical Information Facility
P. O. Box 33
College Park, Maryland 20740

N71-28042

ERRATA

PROTECTIVE COATING SYSTEM FOR A

REGENERATIVELY COOLED THRUST CHAMBER

NASA CR-72855, CONTRACT NAS3-11187, JUNE 1971

Please make the following changes in your copy of the above report: (R-8406)

1. On the top of page 11, the Figure number is 18.

2. On page 96, Eq. (14) should read:

$$\frac{Q_{11-14}}{Q_{4-10}} = \frac{\sum_{11}^{14} \frac{A_w(z)\, h(z)}{h_t}}{\sum_{4}^{10} \frac{A_w(z)\, h(z)}{h_t}} = \frac{0.746}{4.606} = 0.16 \qquad (14)$$

NASA CR-72855
R-8406

PROTECTIVE COATING SYSTEM FOR A REGENERATIVELY COOLED THRUST CHAMBER

Final Report

(1 February 1969 Through 31 December 1970)

By

H. W. Carpenter

Prepared For
National Aeronautics and Space Administration

June 1971

Contract NAS3-11187

Technical Management
NASA Lewis Research Center
Cleveland, Ohio
Chemical Rocket Division
Mr. Charles Zalabak

Rocketdyne
A Division of North American Rockwell
Canoga Park, California

FOREWORD

The effort described herein was performed under Contract NAS3-11187 from 1 February 1969 through 31 December 1970. This work includes two major tasks, Tasks III and IV, out of a total of four that were performed under this contract. Tasks I and II, which were performed from 30 June 1967 through 31 January 1969, were reported in NASA CR-72569. The Technical Manager was Mr. Charles Zalabak, Chemical Rocket Division, National Aeronautics and Space Administration, Lewis Research Center, Cleveland, Ohio 44135. This report is submitted in fulfillment of the requirements of Exhibit B, par. E of the subject contract.

ACKNOWLEDGMENTS

Contributions of the following people are gratefully acknowledged: Mr. T. A. Coultas, Program Manager, Dr. F. C. Gunderloy, Jr., Responsible Engineer, and Dr. S. C. Carniglia, who was Responsible Engineer in the early part of the program; Dr. R. N. Gurnitz, Messrs. J. A. Wrubel, D. E. Hawkins, K. Tate, and C. Nagai for planning and conducting the engine tests, Messrs. J. M. Watkins, B. L. Sorenson, and M. Sternberg for designing and supervising construction of test hardware; Messrs. W. S. Hines, J. G. Gerstley, and R. D. Tobin for heat transfer analyses in regard to designing the engine test hardware; and Mr. J. Testa, Jr. for preparing and photographing the ceramographic mounts.

ABSTRACT

A slurry-applied, heat-barrier coating was developed and evaluated in a planned sequence of arc-plasma jet and rocket motor tests of increasing complexity and severity. The coating, a phosphate-bonded zirconia system, was designed to reduce heat flux through the walls of thrust chambers of liquid hydrogen/liquid oxygen fueled rocket engines from 50 to 20 Btu/in^2-sec and to withstand a 4000 F surface temperature, severe temperature gradients (as much as 10^6 F/inch thickness), and many thermal cycles. Rocket motor tests included:

Chamber Pressure	-	140 to 575 psia
Mixture Ratio	-	6 to 7
Number of Cycles on a Given Specimen	-	1 to 3
Heat Flux Through the Coated Specimens	-	5.0 to 19.2 Btu/in^2-sec

Test specimens consisted of two types: (1) water-cooled, coated single tubes positioned perpendicular to the combustion gas (that actually formed the throat of the rocket motor), and (2) a water-cooled, coated tubular wall in a two-dimensional throat segment.

CONTENTS

FIGURES

TABLES

INTRODUCTION

Advanced liquid-fueled, regeneratively-cooled rocket engines are required as demands are made for higher and higher propulsive effectiveness. The heat flux through the walls of these high-performance engines will be four or five times present levels because of increased chamber pressures. Metals and alloys that are used in current thrust chamber applications are presently near their service limits. Although auxiliary cooling schemes exist (e.g., film cooling), they entail inefficient use of fuel. The amplified pumping demanded for increased regenerative cooling is not satisfactory either, because it lessens efficiency and increases engine weight. To reduce these problems, dependable heat-barrier coatings will be extremely advantageous, if not a necessity.

Use of effective, passive heat-barrier coatings is a means for reducing the heat flux through the walls of regeneratively cooled thrust chambers, and for reducing the service temperature of metal components. Reduced service temperatures will result in extended fatigue life, lower thermal stresses, reduced corrosion rates of metal alloys, and increased flexibility of design. Weight reductions will also result from the decreased heat flux through a decrease in the coolant pumping requirements.

To date, the only successful heat-barrier coatings for rocket engine applications have been applied by melt-spraying methods, the most successful being applied by arc-plasma spraying. While offering several advantages, arc-plasma spraying processes have limitations. Coatings applied by slurry methods offer several potential advantages over melt-spraying methods

Slurry methods require no elaborate, expensive equipment or cooling fixtures. Most importantly, slurry methods are not restricted by substrate size and geometry as they are in arc-plasma spraying. Arc-plasma spraying is a line-of-sight process, and best results are obtained when the coating material is applied at a 90-degree angle to the substrate. Thus, only surfaces that are accessible to the melt-spraying equipment can be coated. Slurry processes, conversely, are not intrinsically limited by size or shape of the part to be coated. Inaccessible surfaces can be coated by dipping the entire part into the slurry or by pouring the slurry into the inaccessible area. Therefore, the most economical and, in some cases, the only feasible coating application technique is one in which the coating is applied as a slurry.

As slurry processes have not yet been used to apply heat-barrier coatings in rocket engines, it was necessary to conduct a feasibility study, which was divided into two major phases. During the first phase (Ref. 1), coatings systems were designed, developed, and then tested with an arc-plasma torch as a heat source. Only cementitiously-bonded systems were considered and, in this report, they will be termed slurry coatings.

The criteria for design and selection of the coating were:

1. Capability of reducing the design heat flux of 50 Btu/in^2-sec to 20 Btu/in^2-sec (gas-side coating temperature must be about 4000 F).

2. Service in high-temperature combustion products of hydrogen and oxygen (oxygen-to-hydrogen weight flow ratio in the range of 5.0 to 7.0).

3. Temperature of metal on the coated side must not exceed 1600 F and the metal must be one of the materials presently used in construction of thrust chambers (e.g., Type 347 stainless steel or Hastelloy-X).

4. Coolant temperatures may range from 50 to 500 R (-410 to 40 F).

For the second phase of the study the most promising coating, phosphate-bonded zirconia, was selected for test in a rocket motor and the results are reported herein. These tests were made on single tubes and then on a more expensive tubular wall configuration. Individual Hastelloy-X tubes were positioned normal to the flow of gases in the throat section of a small hydrogen/oxygen rocket motor. Twenty-one tubes, 17 coated and 4 uncoated, were tested in a total of 9 test firings. Chamber pressure was varied from 142 to 575 psia and test duration in all but two runs was 20 seconds. These tests were preceded by evaluation of identical tube specimens in the arc-plasma jet. The aims of tests on single tubes were to establish coating performance under a range of rocket motor combustion gas environments and to characterize the coating performance as a function of slurry composition, thickness, and chamber pressure. Results would also be used to select coating and motor test parameters for the tubular wall specimen.

For the final test series, a two-dimensional throat section was fitted to the same rocket motor used in the above series. Slurry coated Hastelloy-X tubes formed one wall of the section. Three firings of 20 seconds each were run at 244, 366, and 506 psia chamber pressure. This test and this configuration were representative of a full-scale, advanced engine within the scope of this program.

SUMMARY

A heat-barrier coating system for the gas-side wall of regeneratively-cooled rocket engine thrust chambers was evaluated in a series of rocket motor tests. The coating system is a phosphate-bonded zirconia and was applied as a slurry by air spray techniques to a substrate of Hastelloy X. Design, selection, and preliminary tests were reported previously. In the rocket engine tests, the coating was exposed to high-velocity hydrogen-oxygen combustion products at the temperatures and heat fluxes typical of high pressure rocket engines. The coating successfully withstood surface temperatures of 4000 F and over, temperature gradients of approximately 10^6 F/inch of thickness, thermal shocks from cryogenic temperatures to over 4000 F, and it kept the metal surface temperature to 1600 F or below. Results of these tests indicated that a layer of this coating 3.5 mils thick would provide the thermal performance to reduce the heat flux through the chamber walls of a high pressure engine from 50 to 20 Btu/inch^2-sec.

Two sample configurations were used for the rocket motor tests reported herein. Coated single-tube specimens normal to the gas flow were used in the first series of tests, while the coating was tested on a brazed tubular wall in a two-dimensional throat configuration in the second series. The average heat flux was measured in each case and local values were calculated with theoretical and empirical relations. The local heat fluxes varied over the range associated with flow variation from subsonic to supersonic velocities. Rocket motor test parameters were:

Propellants	-	Hydrogen and Oxygen
Chamber Pressure	-	160 to 590 psia
Mixture Ratio	-	6 to 7

Duration of Each Firing	-	20 seconds
Number of Cycles on One Coated Specimen	-	1 to 3
Average Heat Flux Through the Coated Wall	-	5 to 19.2 Btu/in^2 sec

PROCEDURES

MATERIALS TESTED

As a result of the work done and reported in Ref. 1, phosphate-bonded zirconia was chosen for test in a rocket motor. The compositional range was:

ZrO_2 (-325 mesh)*	10 grams
Binder Solution No. 4 (40 parts by volume 85-percent aqueous H_3PO_4 plus 1 part 60-percent aqueous HF)	0.5 to 1.1 grams
Water (as needed to yield a suitable slurry)	1.5 to 2 grams

Working time of the slurry is about 10 minutes. After 10 minutes, it thickens. More water can be added to thin it, but this practice was avoided because the consequence was unknown. Coatings can be applied by spraying, dipping, pouring, or troweling; they are cured at room temperature, 150 F, and 600 F for 1 hour each.

A significant change in state-of-the-art formulations in the phosphate-bonded ZrO_2 system was made. H_2PO_3F, which is the binder in the state-of-the-art formulation, was replaced by H_3PO_4 plus a small amount of HF. This change eliminated the highly corrosive nature of the existing slurry, which was completely unacceptable for this program, and simplified the chemical system for systematic studies of reactions and application variables.

---

*Zirnorite grade I, CaO stabilized, Norton Company, Worcester, Mass.

The performance evaluation and the optimum slurry formulations were arrived at primarily by arc-plasma jet tests and secondly through other useful laboratory tests. Hastelloy-X was used throughout as the substrate material.

Some selected properties of the phosphate-bonded zirconia are:

Hardness	could not be scratched with a blunt steel probe
Surface Roughness, in. rms	100
Flexual Strength (of cast bars), psi	to 4000
Density$_3$(of cast bars), gm/cm	3.4
Theoretical Density of ZrO_2, gm/cm^3	5.6
Thermal Diffusivity at 1800 F, cm^2/sec	0.002
Efficiency of Thermal Protectiveness	Similar to phosphate-free ZrO_2

Calibration studies and thermal diffusivity measurements indicated that the degree of thermal protection of the phosphate-bonded ZrO_2 coating was similar to that of CaO-stabilized ZrO_2. A coating thickness of 3.5 mils, then, should provide the design thermal resistance.

SPECIMEN PREPARATION

Substrate Preparation

Hastelloy-X substrates were gritblasted and cleaned thoroughly before the coating was applied. Substrates were first cleaned with ethanol or acetone, and then gritblasted with -20 mesh alumina grains to a surface roughness of about 200 microinches rms. The substrate was then cleaned in a trichloroethylene vapor degreaser, rinsed with methanol or acetone, and finally rinsed with ethanol.

Slurry Preparation and Application

Slurry formulations were:

	B44	B45
ZrO_2 (-325 mesh)	100.0 gms.	100.0 gms.
Binder Solution No. 4 (40 parts by volume 85 percent aqueous H_3PO_4 plus 1 part 60 percent aqueous HF)	5.0 gms.	11.0 gms.
Distilled Water	20.0 gms.	15.0 gms.

The mixing sequence was to pour the water into the acid and then pour the binder/water solution into the ZrO_2 powder. The slurry was mixed manually with a polyethylene blade for about one minute. One-hundred-gram batches were made and then used immediately after mixing. Thus, the slurry was always applied on the specimen substrate within 5 minutes after mixing. Slurry B45 was always used unless stated otherwise.

The slurry was sprayed on the specimen substrates using a conventional paint spray gun*. Bottled nitrogen gas was used to pressurize the spray gun. Gas pressure was varied from 45 to 60 psi and spraying distance was varied from 6 to 10 inches. Thickness uniformity was difficult to control because the spray pulsated and because the coating usually had to be applied on a single pass over the substrate. More than one pass resulted in excess thickness, and longer spraying distances resulted in a rough coating texture. Rough surfaces are undesirable because the high spots cause hot spots and turbulence during testing. The desirable condition was to apply a smooth, wet layer of slurry on the specimen substrate in the single pass.

Single and double tube specimens were sprayed with axial traverses of the spray gun. Single tubes were rotated about a one-quarter turn after each traverse of the spray gun. Initially, single tubes were sprayed while rotated in a drill chuck, but this was found to have harmful effects on the performance of the coating, as described in another section. The tubular wall throat segment was coated twice. The original coating was stripped off by gritblasting. The second was applied with two passes of the spray gun, one pass over the upstream straight section of tubes and one pass over the downstream straight section of tubes.

The first coating had to be removed because two of the Hastelloy-X tubes were accidentally damaged by pouring water through the tubes too soon after the liquid nitrogen prechill operation (described below). The water froze and the ice burst open two of the tubes in the straight downstream section of the tube wall. The cracks were repaired with 82 Au-18 Ni braze alloy using a tungsten-inert-gas welding unit. The brazed zone was carefully filed back to the original tube contour. The repaired zone, including the entire tubular wall, was gritblasted and

*Model 15, Binks Manufacturing Company, Chicago, Illinois

recoated in the same way as before. Thus, the coating was tested on a repaired tube substrate in two locations (Refer to Figure).

Liquid Nitrogen Prechill

All tube specimens including the Task IV tubular wall throat segment were prechilled with liquid nitrogen before testing. This was done to simulate the liquid hydrogen prechill in liquid hydrogen/liquid oxygen rocket engines. The tubes were plugged at one end and filled with liquid nitrogen. The liquid nitrogen was replenished as it boiled out so that each tube was chilled for a duration of two minutes. In the case of the tubular wall in the two-dimensional throat segment, the hardware was simply inverted so that the liquid nitrogen could be poured through one of the manifolds into the tubular wall. The tubular wall was also prechilled two minutes. Two minutes of prechill was sufficient for about 1/8 inch of frost to form over the coating from moisture in the air. When the frost melted later, the coating was saturated with water. This water was simply allowed to air dry.

Coating Thickness Measurement

Coating thickness on the single tube specimens used in the first series of rocket motor tests was determined by measuring the O.D. of the tubes with a micrometer in several locations before and after the coating was applied. This procedure was tedious and, it turned out, unreliable. A more satisfactory method was to use a nondestructive measurement based on eddy current phenomena*. Accuracy of these measurements was checked by destructive analysis, but true thickness was difficult to measure, even by destructive methods. Specimens were sectioned

---

*Dermitron Instrument, Unit Process Assemblies, Inc., New York, N. Y.

perpendicular to the axis at the location that was measured using the eddy current instrument. These sections were mounted and prepared for microscopic examination. Thickness was measured at high magnification using a filar eye piece, but the boundaries of the coating were difficult to determine accurately. This was due to the irregular contour of both the gritblasted Hastelloy-X substrate and the coating surface. A calibration study showed, nonetheless, that the differences in measured thicknesses between the two methods was relatively small. Largest differences in measured thicknesses were:

1.	At a single location	1.1 mil
2.	Average of eight locations on a single tube	0.6 mil
3.	Average of a total of 64 locations on 8 different tubes	0.2 mil

Considering that the destructive method yielded "true"thickness values, then a measured value in a single location using the NDT instrument could be about 1 mil in error, but the average of several measurements in different locations would be accurate within 0.6 mil or less.

This instrument, unfortunately, was very inaccurate for measuring coating thickness on the smaller tubes in the brazed tubular wall in the two-dimensional throat segment. Considerable scatter in the readings probably was caused by the smaller diameter of the tubes plus the effect of the braze fillet.

Thickness was indirectly measured on two glass slides that were positioned adjacent to the tubular wall, like wings, during the spray-coating process. The glass slides were coated on the same passes of the spray gun as the tube wall. Thickness was measured with a standard micrometer. Thickness of the coating on the tube wall also was measured directly at two locations using a micrometer with a four-inch opening. Accurate measurements were not possible in other locations due to the irregularity of the backside.

ROCKET MOTOR DESCRIPTION

A unique rocket motor that was previously designed and built at Rocketdyne on IR&D funds to test coated refractory tubes at high heat flux and shear conditions was employed. The complete rocket motor assembly is shown schematically in Figure 1. The water-cooled motor incorporates a removable throat section containing three 3/8-inch diameter tubes with a wall thickness of 0.015 inch (Figure 2). Exposed length of the tubes is one inch. The entire throat section can be removed after each test and replaced with another throat section containing different tubular specimens. The tubes, which were internally cooled with water, are normally easily removed, facilitating an alternate rapid replacement method. This procedure allows several tests to be run on different tube specimens in a single day of testing with the same engine so that complicated, intermittent scheduling of the test stand facilities is not necessary. External (hot-side) wall temperature and heat flux through the wall can be controlled by variation of a number of parameters, including chamber pressure, coating thickness, coolant pressure, and flowrate. In this way, the same coating system can be tested under different heat flux conditions during the same test run. This degree of control also permitted individual monitoring of coolant conditions through each tubular specimen.

A 14-element gas-on-liquid triplet injector was utilized. Although the injector (Figure 3) was originally designed and tested with LF_2/GH_2, modification to the LOX/GH_2 propellant combination was easily accomplished by enlarging the fuel side orifices. Ignition was accomplished by injecting a small quantity of gaseous fluorine during the fuel lead just prior to oxidizer valve actuation.

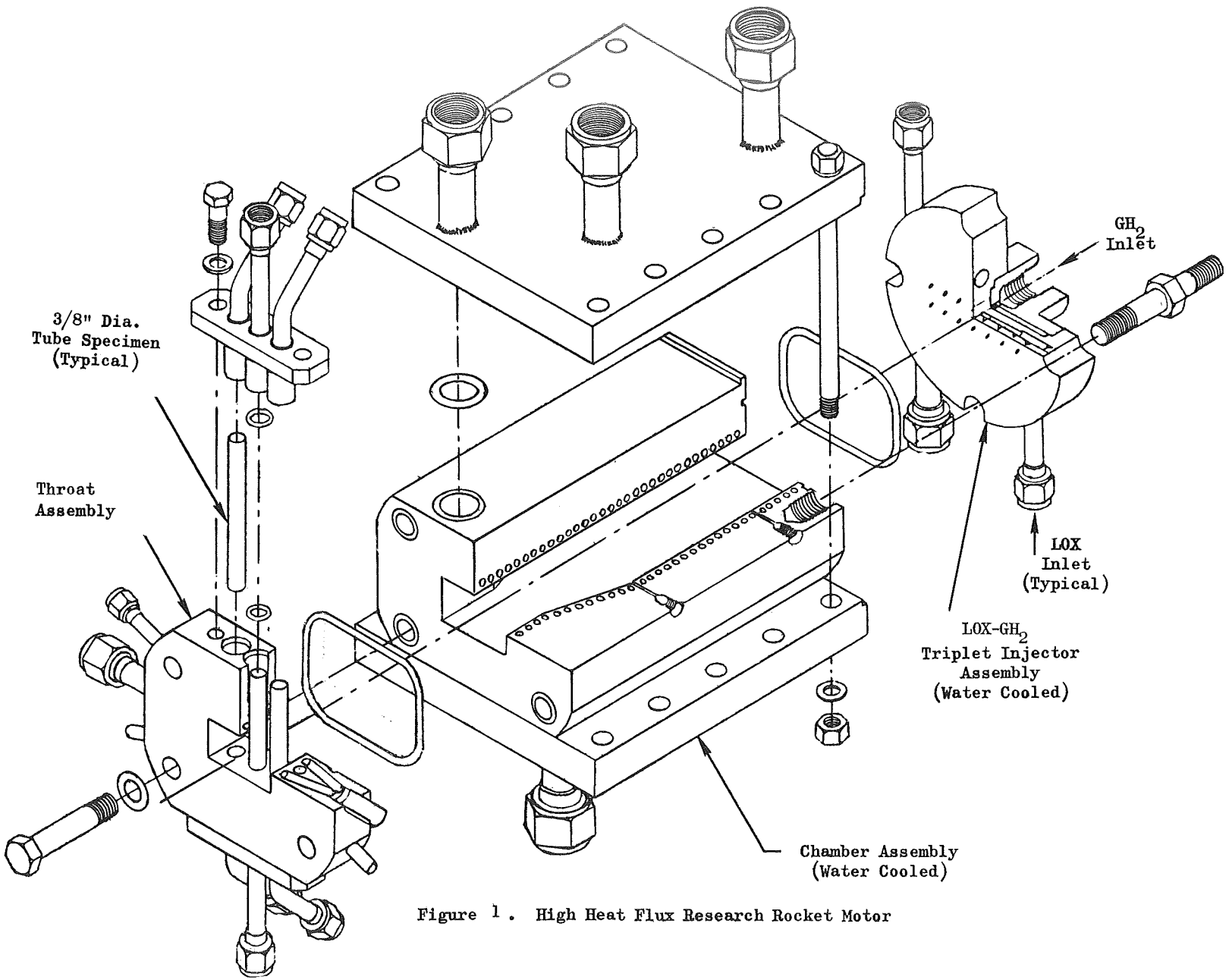

Figure 1. High Heat Flux Research Rocket Motor

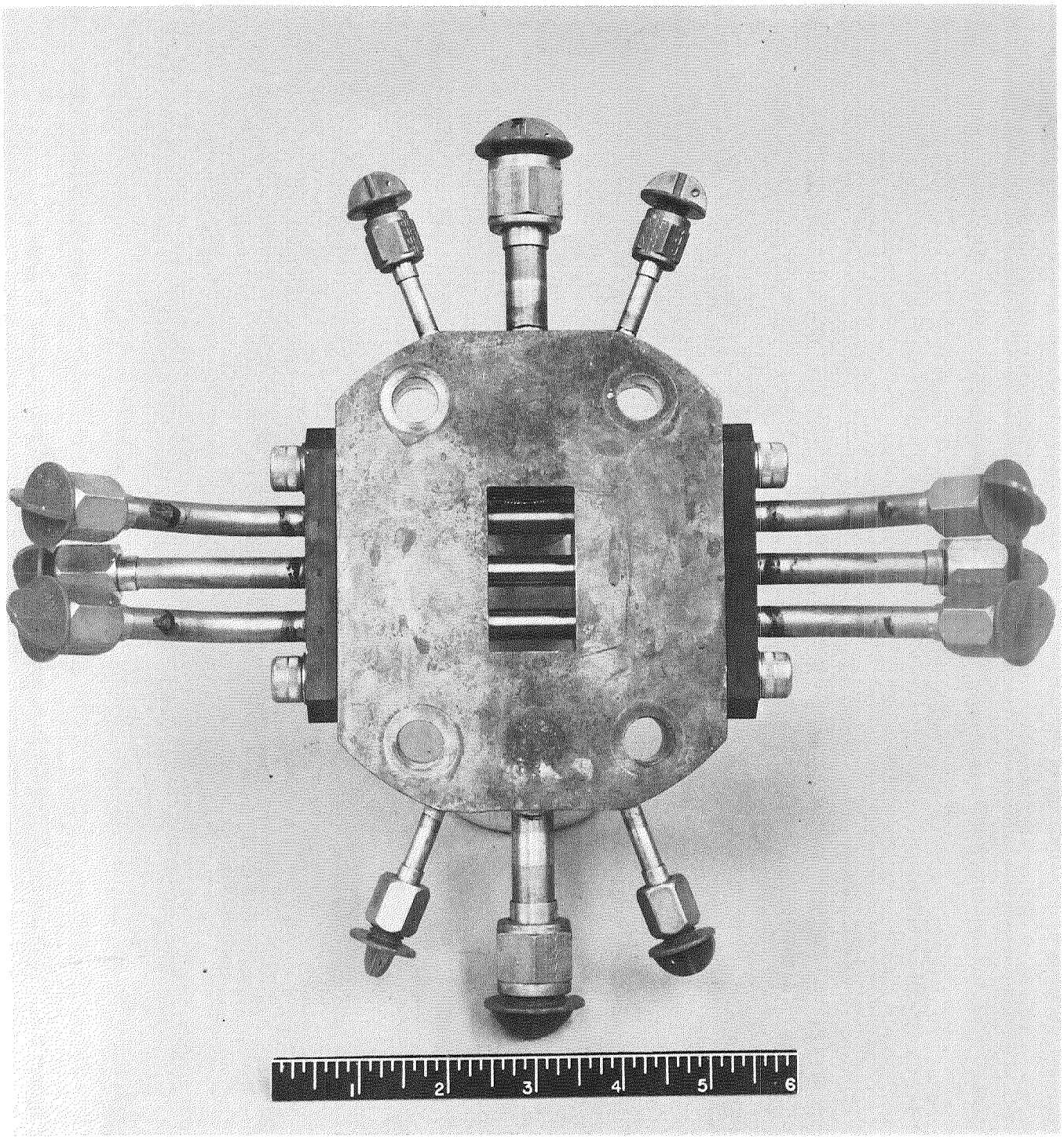

5AA33-3/24/67-S1

Figure 2. Throat Segment Containing Three Uncoated Tubes

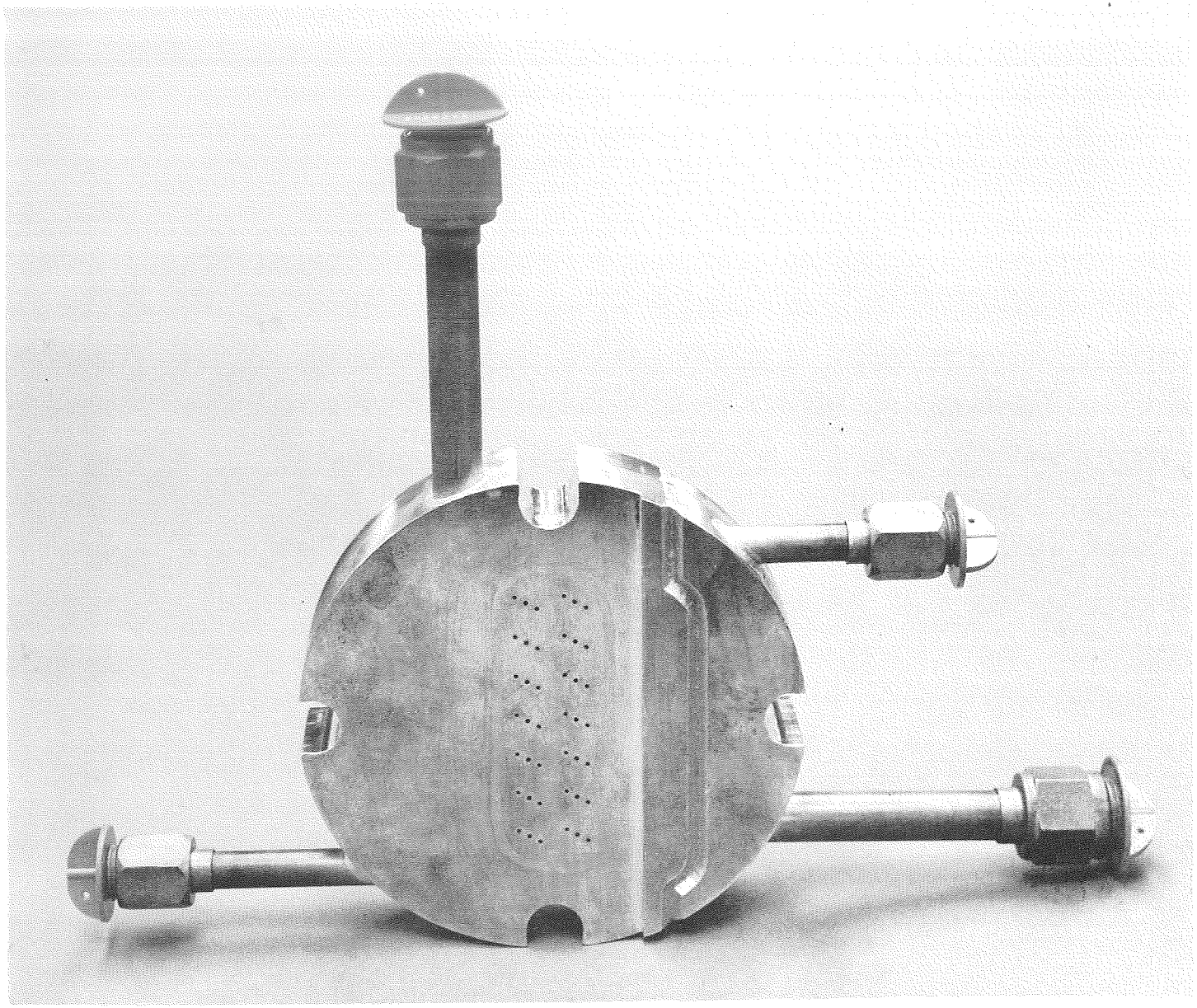

5AA36-2/13/67-S1A

Figure 3. 14-Element Triplet Injector for the Small Test Rocket Engine

ROCKET MOTOR TEST FACILITY

Test facilities that were used for the rocket motor firings are located in the Propulsion Research Area, Area I, at Rocketdyne's Santa Susana Field Laboratories in Chatsworth, California. Major facility items included:

1. Engine mount
2. Propellant delivery lines and valves
3. 110 gallon, 3000 psi, LOX tank
4. 3800 gallon, 3000 psi, hydrogen bottle bank
5. 800 gallon, 2500 psi, water tank
6. GF_2 ignition system
7. 2200 gallon, 44 psi, community LN_2 sphere
8. GN_2 source for purging and pressurization

The oxygen lines were LN_2 chilled and the injector was conditioned by LOX flow prior to the test-sequence start to assure liquid oxygen flow during mainstage. The gaseous hydrogen was delivered at ambient temperature from a high pressure storage bottle bank. The water coolant lines provided both a coolant source to prevent hardware failure and a calorimeter data source for heat flux determination.

Test Instrumentation

Instrumentation consisted primarily of standard pressure transducers, turbine flowmeters and thermocouples. LOX flowrates were determined with flowmeters, while GH_2 flowrates were calibrated with a venturi in conjunction with line pressure and temperature measurements. Chamber pressure, which was determined redundantly, was used to calculate a

nominal characteristic velocity efficiency. Calorimetric heat flux data were taken from measurements of water flowrate and temperature rise using 3- and 4-element thermopiles.

Electrical outputs from test stand instrumentation were delivered to the blockhouse control center. Critical parameters were reproduced visually on data monitoring recorders (for immediate test interpretation), while all parameters were relayed through a Beckman Model 210 Data Acquisition Recording System to a permanent tape from which computer data reduction and scaling were accomplished. Instrument calibrations were conducted periodically to assure high quality data.

DESCRIPTION OF THE TUBULAR WALL, TWO-DIMENSIONAL THROAT SEGMENT

A throat segment with a tubular wall was designed and built for test firing in the same motor used for the individual tubes. The cross section of the throat was rectangular, 1.90 inches wide by 0.4 inch from the copper wall to the crowns of the Hastelloy-X tubes (Figure 4). By design, it had approximately the same cross-sectional area as the throat formed by the single tubes tested in Task-III. The tube-wall side was made of ten Hastelloy-X tubes, 0.190 inches O.D. with an 0.015-inch wall thickness, that were contoured individually and then brazed in the copper tubular-wall block assembly (Figures 4 and 5). Four braze cycles were required. The first was at 1910 F for 10 minutes using Nicoro braze (62 Cu-35 Au-3 Ni); the second, third, and fourth were at 1820 F for 10 minutes using a 50 Cu-50 Au braze alloy. All brazing was in a hydrogen atmosphere, and the braze did not seem to migrate over the tube crowns. Both ends of the tubular array protruded into large holes, or manifolds, that were drilled crosswise in the copper block (Figure 6). The ends of the manifolds on the side of the assembly were sealed by brazed copper plugs (Figure 7). The gaps formed by the interstices of the tubes where they went into the copper block also were filled with braze alloy (Figure 5).

The tubular-wall block assembly was not inserted into the copper sidewalls until after the coating was applied and cured. The reason was so that the coating could be sprayed on at right angles in the same way that it was sprayed on specimens in the preceding phases of the program. Had the coating been applied by dip-coating or by pour-coating methods, the coating thickness could not have been sufficiently controlled within the state-of-the-art.

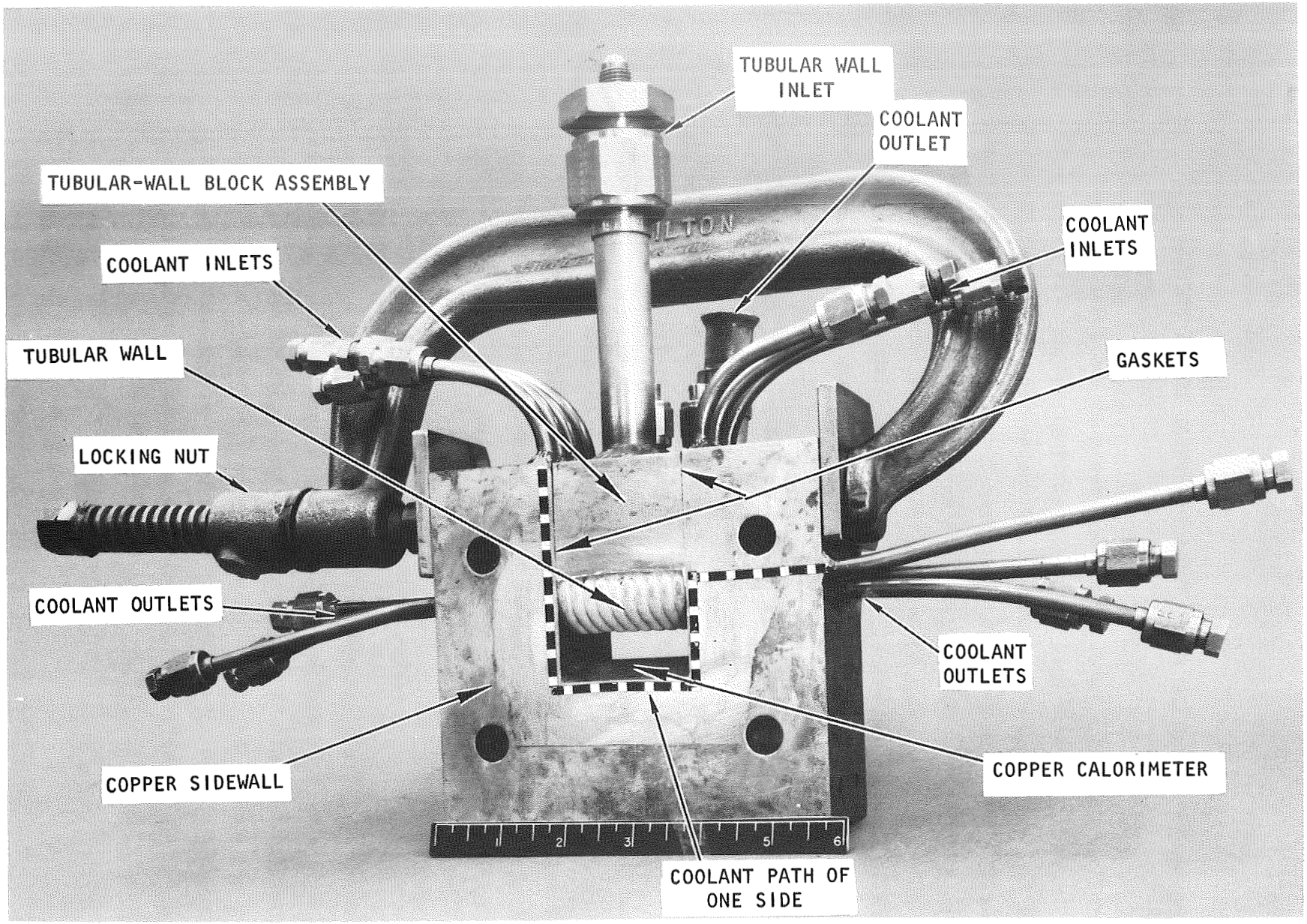

1XZ32-6/18/70-C2D

Figure 4. Two-Dimensional Throat Segment: Upstream Side

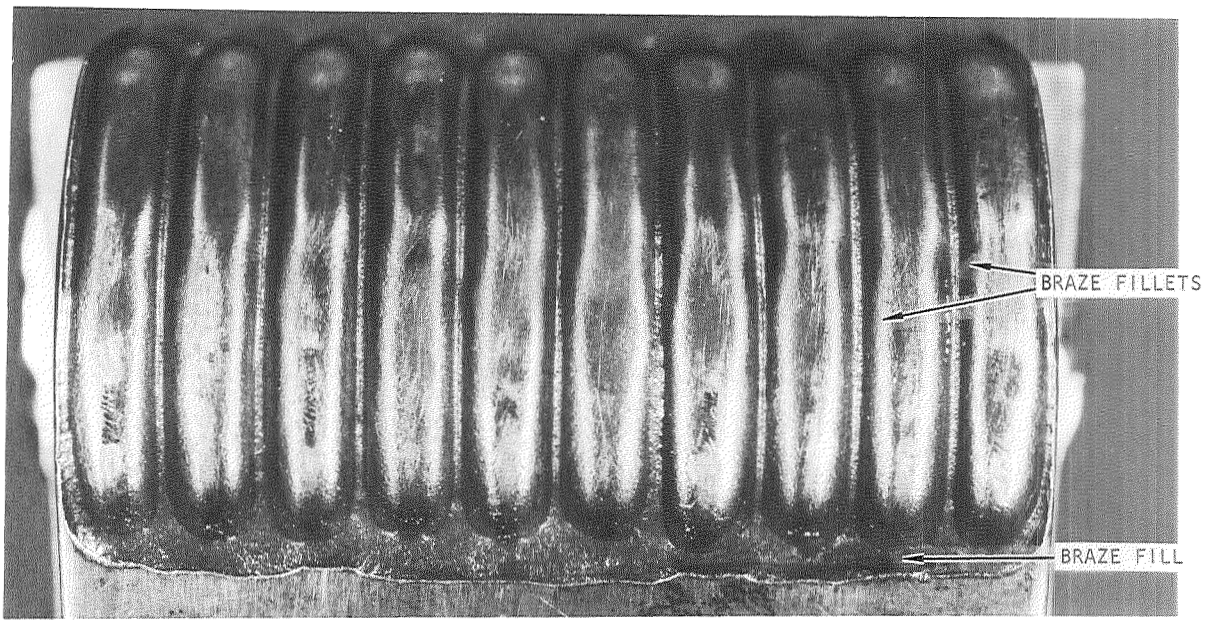

5AE13-6/1/70-C1A

(a) Upstream End: Front View

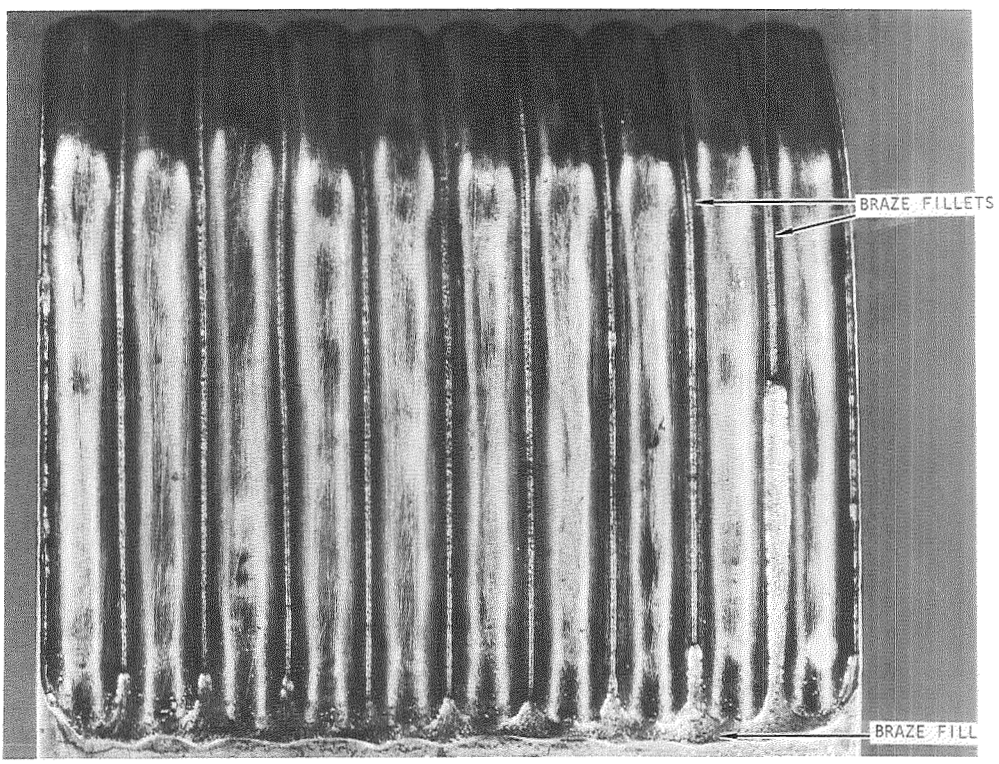

5AE13-6/1/70-C1B

(b) Downstream End: Top View

Figure 5. Views of the Uncoated Tubular Wall Showing the Brazed Fillets

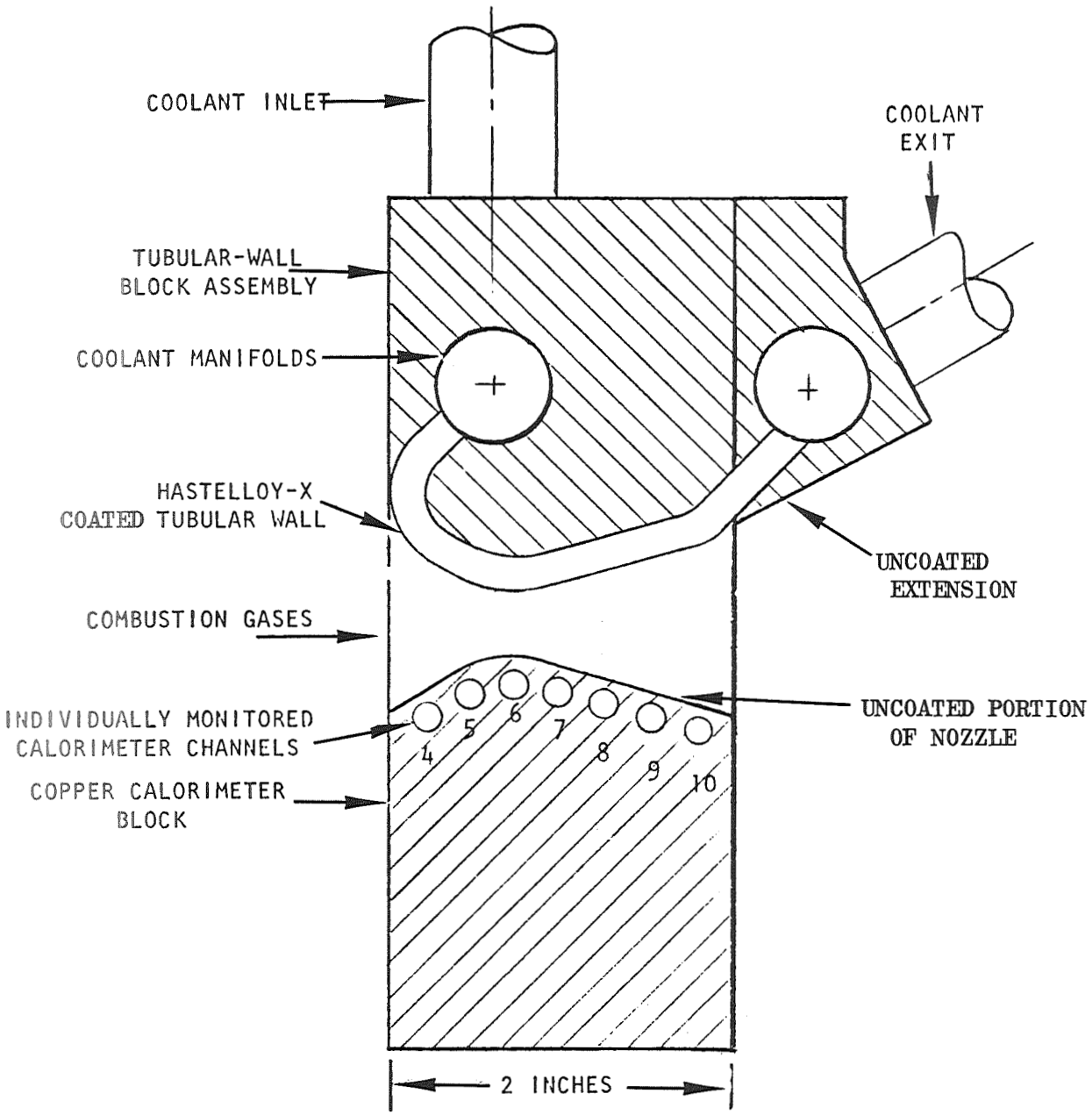

Figure 6. Cross Section of the Two-Dimensional Throat Segment

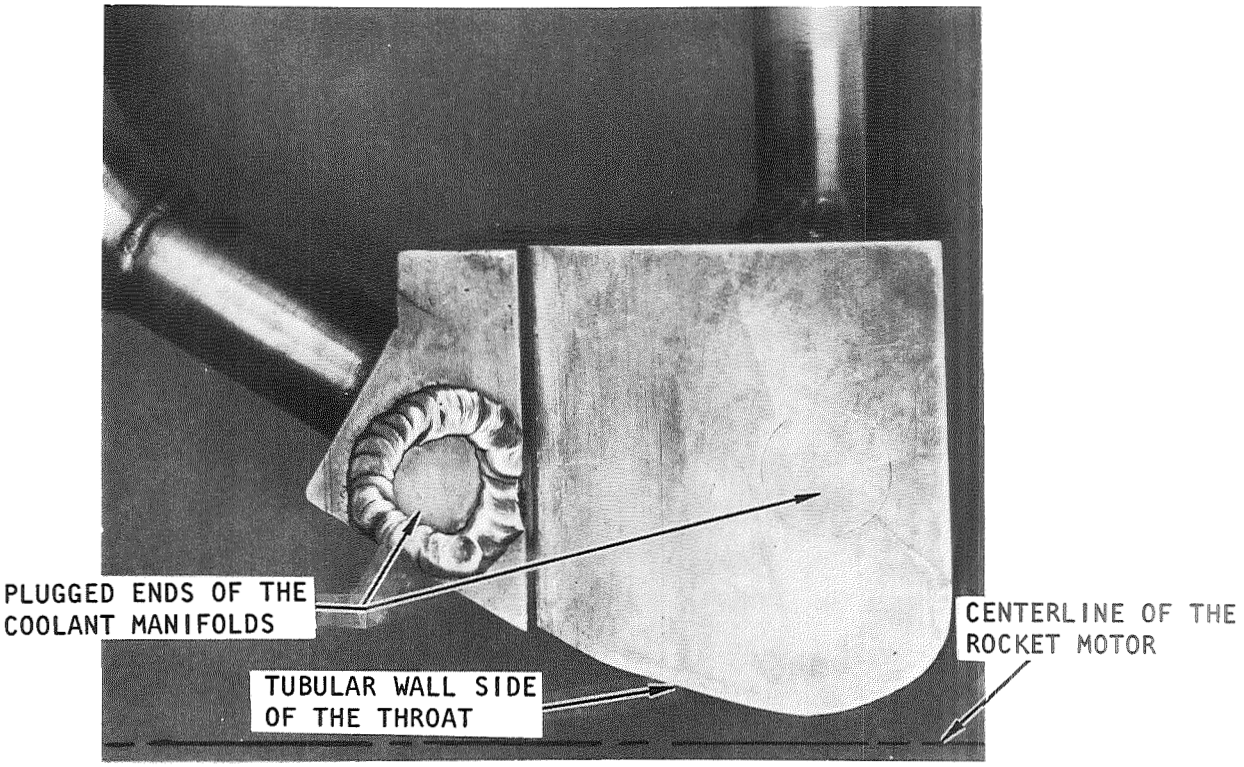

5AE13-6/1/70-C1C

Figure 7. Side View of the Tubular-Wall Block Assembly

The tubular-wall block assembly was not brazed to the copper sidewalls because adherence of the coating to the substrate is damaged by a high-temperature anneal under isothermal conditions (Reference 1). Frictional forces, thus, were used to hold the throat insert in place during test firing. Rubberized asbestos gaskets, 12 1/2 mils thick were used to seal the sides of the tubular-wall block assembly to the copper sidewalls and the required frictional force was provided by an ordinary C-clamp (Figure 4). The design torque was applied to the C-clamp and a special locking nut was used to keep the C-clamp from loosening during testing. This torque, which was checked after each firing, did not change, and the tubular-wall block assembly did not move even a fraction of an inch during the three consecutive firings.

The tubes forming the tubular wall were not formed to close tolerance because it was not necessary for evaluation of the coating or for performance of the hardware. Consequently, the tube crowns protruded beyond the face that bolted flush to the combustion chamber. To prevent smashing the tube crowns and damaging the coating when it was installed, a recessed area was milled in the mating face of the combustion chamber (Figure 8). Each side of the throat opening was milled so that the two-dimensional throat segment could be attached either way, i.e., upside down, or right side up.

The opposite wall of the throat was a water-cooled copper calorimeter. Seven coolant holes were drilled laterally along the throat contour (Figure 6). Each passage was monitored so that a heat-flux profile along the throat could be obtained for each test firing. The flow path of one coolant passage through the calorimeter is drawn in Figure 4 . Four such passages were located on one side, while three were located on the other side. The outlet line was designed on the side rather than on the top because there was not enough room to weld all seven steel tubing lead-ins on a single surface.

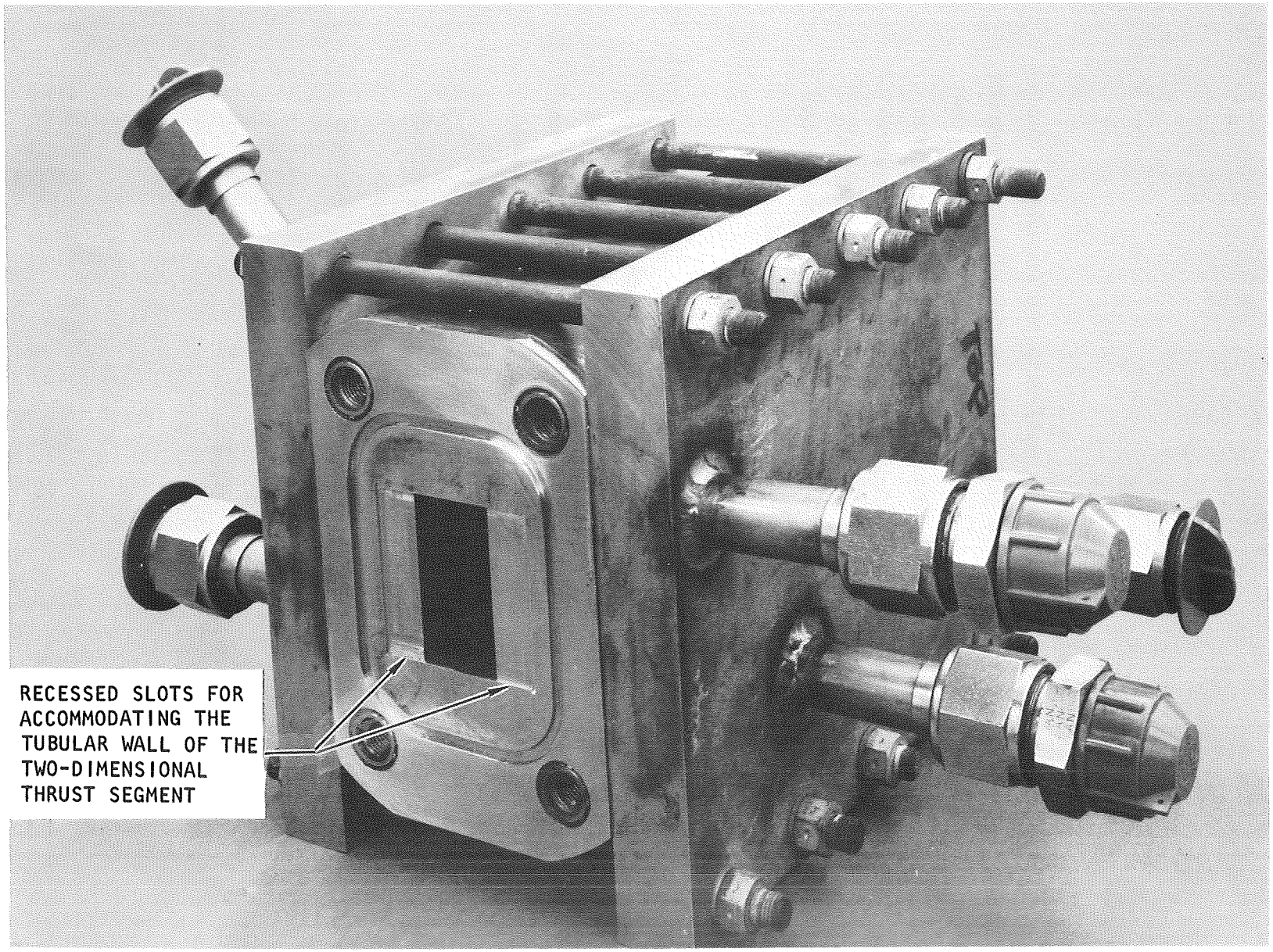

1XZ32-6/18/70-C2B

Figure 8. Combustor of the Two-Dimensional Motor Showing the Face That Mated With the Throat Segment

ARC-PLASMA JET TEST

Several tests of a verification nature were made with the arc-plasma torch as heater. The rocket motor tests were to be made on coated tubes, whereas the tests reported in Ref. 1 were made on flat specimens. Because of the difference in geometry, it was considered necessary to verify the chosen coating composition and preparation on tubular specimens. The procedure used in these arc-plasma jet tests was the same as that used in Ref. 1. Water-cooled coated tubes were heated by the plasma torch to an indicated surface temperature and were then moved in and out of the plasma flame. Heating and cooling were essentially instantaneous.

Properly applied on the tubular specimens, the coating survived 25 cycles from the indicated temperature of 4000 F to 60 F plus about 5 minutes at 4000 F. Thus, it was shown that the tubular geometry did not negate conclusions of coating capability derived from tests on the flat specimens.

Both single- and double-tube geometries were tested. The substrates were 3/8-inch diameter Hastelloy-X tubes with 0.015 inch wall. The double-tube specimens were made by joining two of these tubes by electron-beam weld or braze (Fig. 9). The braze alloy was AMS 4777:

Element	Nominal Wt. %
Ni	82
Cr	7
Si	4.5
Fe	3
B	2.9

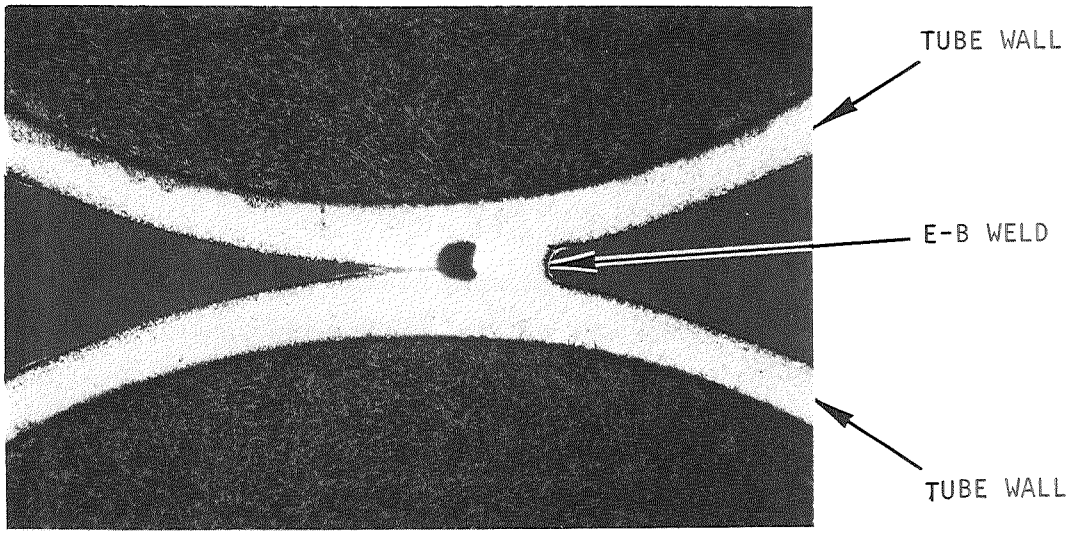

Figure a. Electron-Beam Weld Between Two Hastelloy-X Tubes (0.015 Inch Wall Thickness; Mag X25)

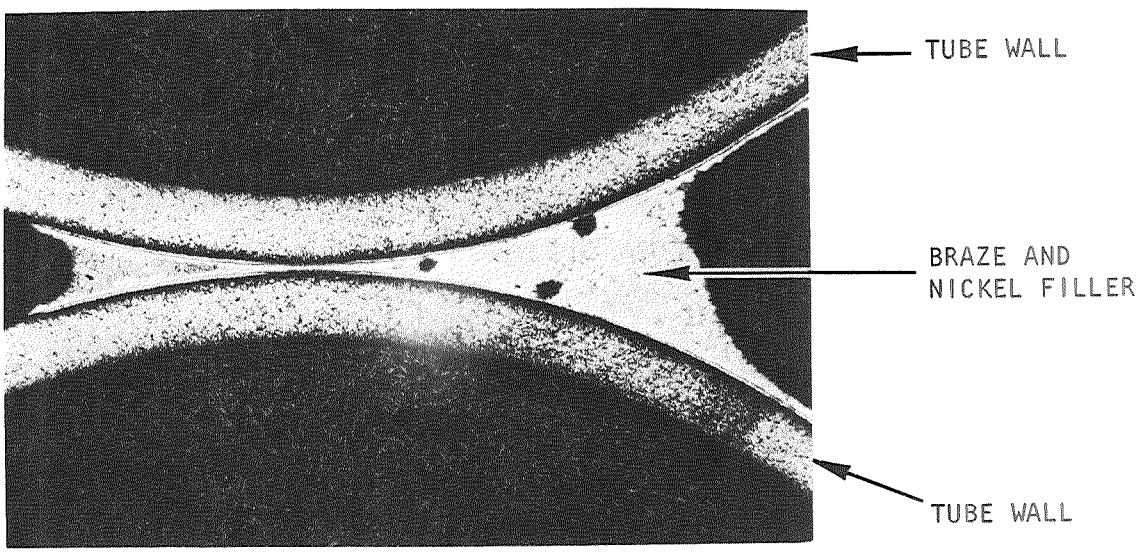

Figure b. Brazed Zone Between Two Hastelloy-X Tubes (0.015 Inch Wall Thickness; Mag X25; 10% Oxalic Acid-Electrolytic Etch)

Figure 9. Joined Zones of Tube Pair Type of Specimen

The valley between the tubes was filled with nickel powder before the braze alloy was applied, and the braze was applied on one side only. Brazing temperature was 1950 F for 1/2 hour.

The initial arc-plasma jet tests on the single-tube specimens indicated a problem: many tiny hot spots formed on the surface of the coating and, consequently, portions of the coating melted and spalled. Microscopic examination of the specimens before and after testing pointed out the reasons for the poor results.

Three microstructural features were atypical compared to coatings previously tested. One was exaggerated variations in thickness that caused the hot spots during testing. With constant heat flux provided by the arc-plasma jet, local surface temperature could increase hundreds of degrees Fahrenheit due to the gross increase in thermal resistance across the specimen. The thickness variations were traced to two causes. One was a higher degree in surface roughness of the Hastelloy-X substrate (210 to 280 compared to typically 150 to 220 microinches rms; also see Fig. 10), while the other cause was the rough surface texture of the coating (Fig. 11). Cause of the rough surface texture was due to spraying technique. In an attempt to improve uniformity in coating thickness, the spraying distance was increased. Consequently, the slurry was partially dried by the time it deposited on the substrate. Both of these causes in thickness irregularities were simple to rectify. The air pressure during the grit blasting operation was reduced, and the spraying distance was reduced to deposit a wet coating which, when dried, resulted in a smooth surface texture.

The other atypical microstructural feature was a concentration gradient of zirconia grains in the coating, with the lowest population near the interface (Fig. 10). The high porosity at the interface caused a weak stratum in the coating that readily failed during thermal cycling, i.e., the coating fractured at the coating/metal interface. The cause of this phenomenon was the centrifugal forces on the zirconia grains as the tube was rotated in a drill chuck during the spraying process. Rotating the tube while spraying the slurry on it was abandoned.

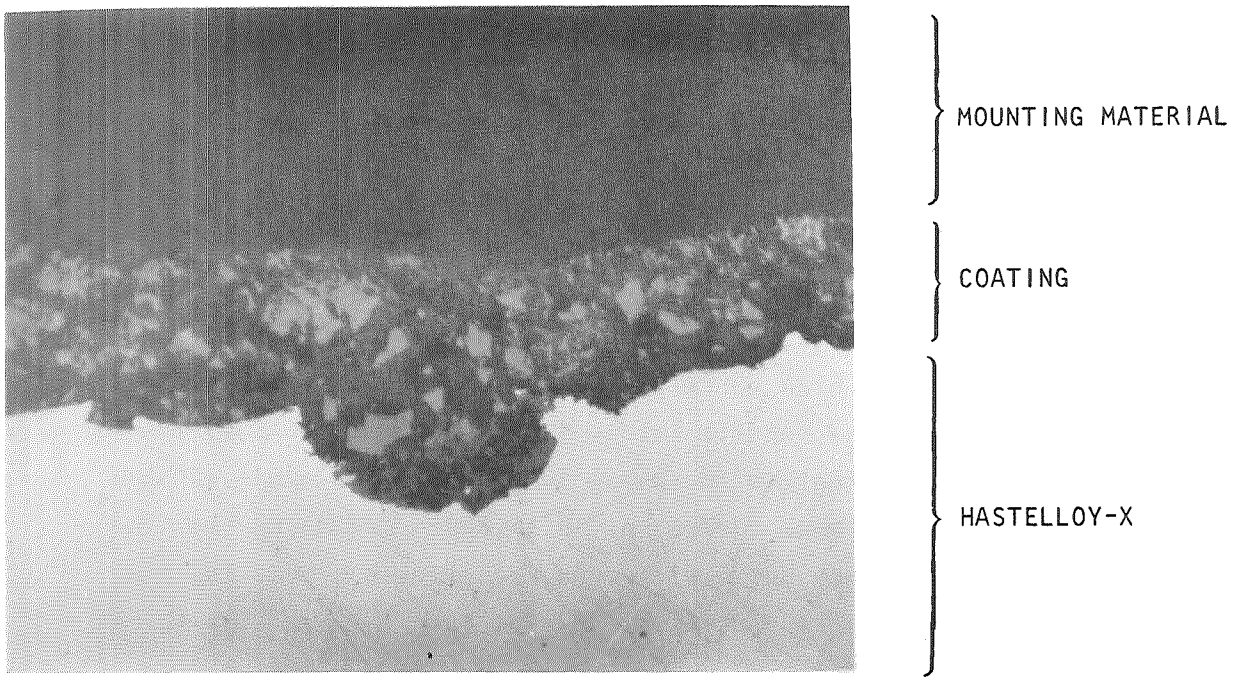

(a)

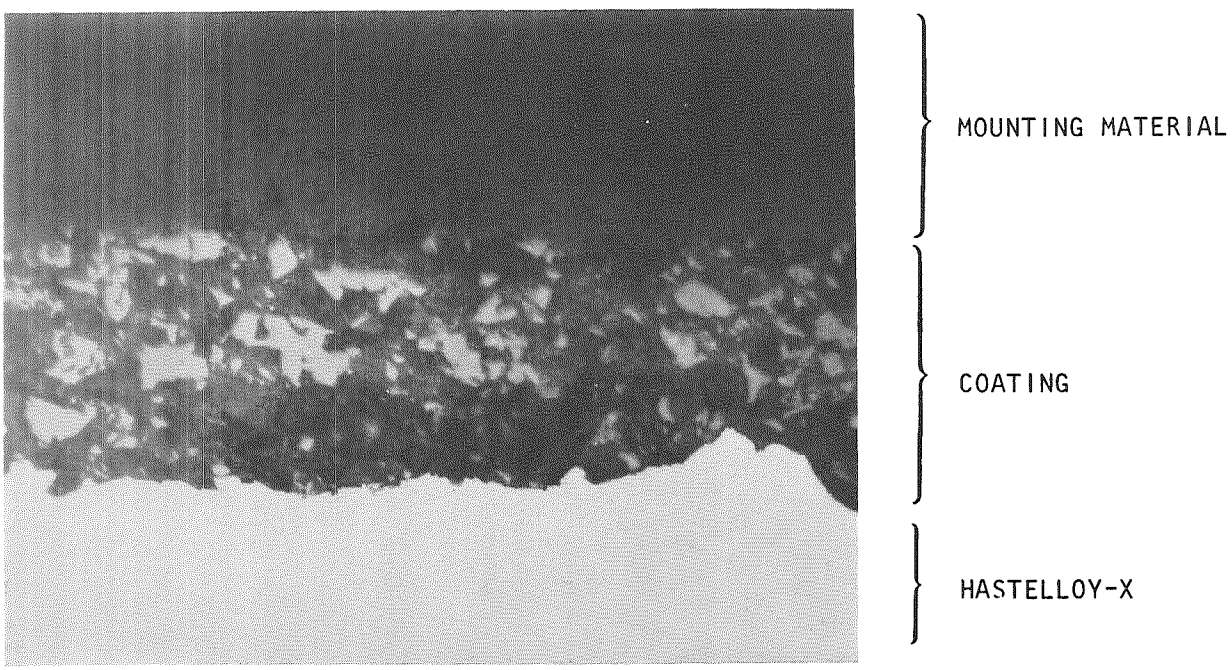

(b)

Figure 10. Microstructure of Untested Areas in Specimen 5 Showing: (a) Local Thickness Variation, (b) Weakened Structure Near Interface (Mag X400)

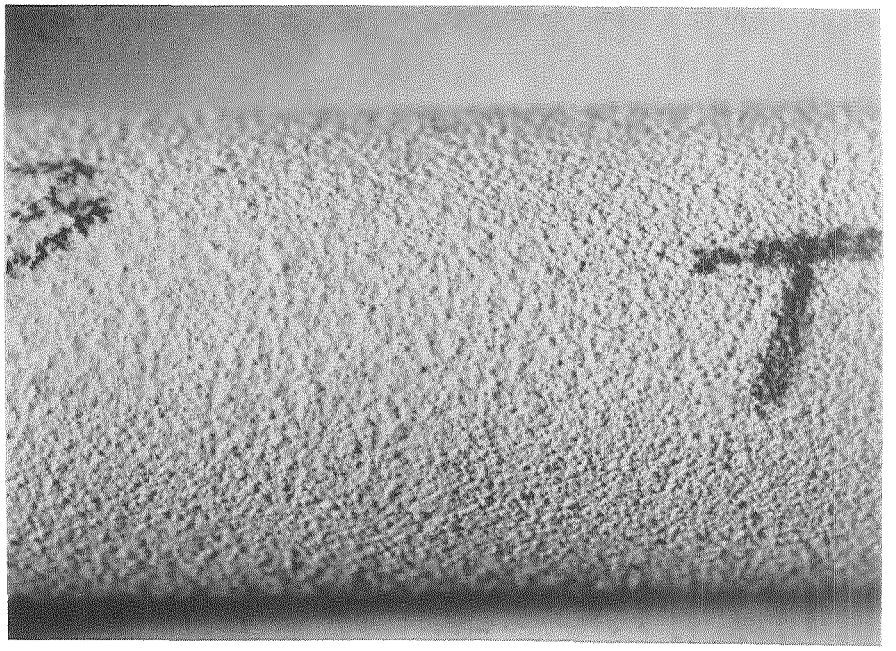

5AG15-9/19/69-C1F

Figure 11. Untested Coating Surface Showing Rough Texture. Magnification X7.

RESULTS AND DISCUSSION

ROCKET MOTOR TEST RESULTS: INDIVIDUAL TUBES

A series of rocket firings was made to test individual tube specimens. It consisted of three firings (runs 52, 53, and 54) plus two preliminary checkout firings (runs 50 and 51). Tests were conducted at a mixture ratio of 6, over a chamber pressure range of 288 to 575 psia, for test durations of 20 seconds for each run. Pertinent test parameters for the series, including rocket operating conditions, slurry type, average coating thickness and heat transfer results are listed in Table I. The details on heat transfer calculations are given in Appendix A.

Evaluation of the test results was encouraging. The heat transfer through the tube wall was reduced by as much as 40%. Calculated theoretical peak heat flux through coated specimens in the series bracketed 20 Btu/in^2-sec. Theoretical peak coating surface temperature was calculated to be 4000 F or higher in some specimens and it was estimated to be even higher based on microscopic examination. Microstructural features, as compared to prior results in arc-plasma tests, indicated that peak coating surface temperatures were above 4000 F in all specimens.

The coating performed exceptionally well in the region from the upstream stagnation to the point of gas flow separation. It did not spall or degrade by reaction with the combustion gas. Downstream of the separation point the coating spalled extensively, probably due to substrate deformation in this region. Some fusion and flow was evident; however, the coating apparently stabilized shortly after the beginning of the test and no measurable erosion was observed.

TABLE I

INDIVIDUAL TUBE TEST RESULTS

Stand Run No.	Chamber Pressure (psia)	Mixture Ratio (O/F)	η_{c*} Uncorrected %	Tube Position(1)	Specimen Number	Slurry Composition	Avg. Coating Thickness (Mils)	Nominal Test Duration (sec.)	Avg. Measured Heat Flux (Btu/in^2-sec.)	Calc'd Peak Heat Flux (Btu/in^2-sec.)	Corrected Measured Ave. Heat Flux $\frac{Q/A}{\eta_{c*}}$ (2)
50	288	6.69	94.5	(Left)	--		0.0(3)	3.0	19.2	--	21.5
50	288	6.69	94.5	(Center)	12	B45	1.7	3.0	15.0	--	16.7
50	288	6.69	94.5	(Right)	10	B45	2.7	3.0	12.4	--	13.9
51	294	6.20	97.0	1	--		0.0(3)	20.0	18.1	32	19.2
51	294	6.20	97.0	2	10	B45	2.7	20.0	16.0	--	17.0
51	294	6.20	97.0	3	12	B45	1.7	20.0	13.7	--	14.6
52	302	6.30	96.7	1	34	B44	2.0	20.0	17.9	20.8	19.1
52	302	6.30	96.7	2	22	B45	2.4	20.0	16.0	19.4	17.1
52	302	6.30	96.7	3	26	B45	3.3	20.0	15.1	17.2	16.1
53	442	6.12	99.0	1	18	B45	3.1	20.0	13.3	20.1	13.6
53	442	6.12	99.0	2	35	B44	1.9	20.0	17.4	22.2	17.8
53	442	6.12	99.0	3	23	B45	2.5	20.0	17.8	25.0	18.2
54	575	6.00	99.5	1	25	B45	2.6	20.0	19.1	26.7	19.3
54	575	6.00	99.5	2	28	B45	2.7	20.0	16.3	24.9	16.5
54	575	6.00	99.5	3	32	B44	1.7	20.0	15.2	23.5	15.4

(1) Viewed toward the Injector

(2) Area 1.215 in^2

(3) These tubes were actually coated with up to 2 mils of alumina

Macroscopic Examination. Figures 12 through 15 show each test specimen in the posttest condition in front, side and rear views. Significantly, no spalling occurred, nor was erosion or any detrimental chemical reaction apparent in the test zone of the front face of any specimen (Figs. 12a, 13a, 14a, and 15a). The spalling seen in specimens 25, 28, and 32 (Fig. 14) occurred during removal from the throat fixture. Specimens 25 and 28 had to be sawed out while specimen 32 was physically forced through the entry hole. The difficulty in removal was caused by bowing of the tubes during testing. Bowing of the tube to this extent undoubtedly subjected the coating to untypically high stresses, particularly on the downstream side where the coating was placed in tension.

Some surface fusion was apparent in all specimens when viewed at a magnification of about 5X. The fused coating flowed along the sides of the tubes in narrow straight lines perpendicular to the tube axis. It also flowed into the annulus over the untested coating where the tube specimen entered the throat fixture (note particularly the ends of specimens 22 and 26 in Fig. 12a).

The coating on the front face appeared darkened after testing, mainly due to the formation of small black marks. The marks seemed to be of two kinds: (1) surface stains which formed smears and wavy lines (see Fig. 12a, specimen 34), and (2) spots which appeared to penetrate into the coating.

These black spots were similar to those observed in a coating that was tested in the arc-plasma jet using an argon/5% hydrogen mixture. Oddly, the darkest coloring occurred in specimens tested at 442 psia, not at 575 psia.

Inspection of the sides of the specimens (Figs. 12b, 13b, 14b, and 15b) also show that there was no spalling, erosion, or detrimental chemical reaction. Two significant features are readily apparent in these views. First, the point of gas flow separation is shown by the sharp edges of colored areas and by the abrupt end of the flow lines of fused coating. Color of these darkened areas was black and burnt sienna. The black smears originating at the ends of some test specimens are due to burned gaskets. Second, when spalling occurred on the downstream side of the specimen, it stopped where the gases separated from the coating surface. This is most apparent in specimen 26 (Fig. 12b and c) where downstream spalling was greatest.

The downstream side of the specimens, which was away from the combustion chamber and exposed to the atmosphere*, were stained in various shapes and shades of black, lavender, burnt sienna, and copper color (Figs. 12c, 13c, 14c, and 15c). Spalling occurred on the downstream side of the specimens with the thickest coating. As pointed out before, the spalling stopped where the gas stream separated from the tube. Spalling was greatest in the first test at the lowest chamber pressure (specimen 26, Fig. 12c). Most of the Hastelloy-X substrate exposed by this local spalling was covered with fragments of attached coating, indicating that there was good adherence. Small significance is given to spalling because the

* There was no nozzle; the rocket engine ended at the throat.

Figure 12. Coated-Tube Specimens After Rocket Engine Test at P_c = 302 psia. Magnification X4-1/2.

(a) Front: The Surfaces Facing the Injector.

5AG15-9/25/69-C1H

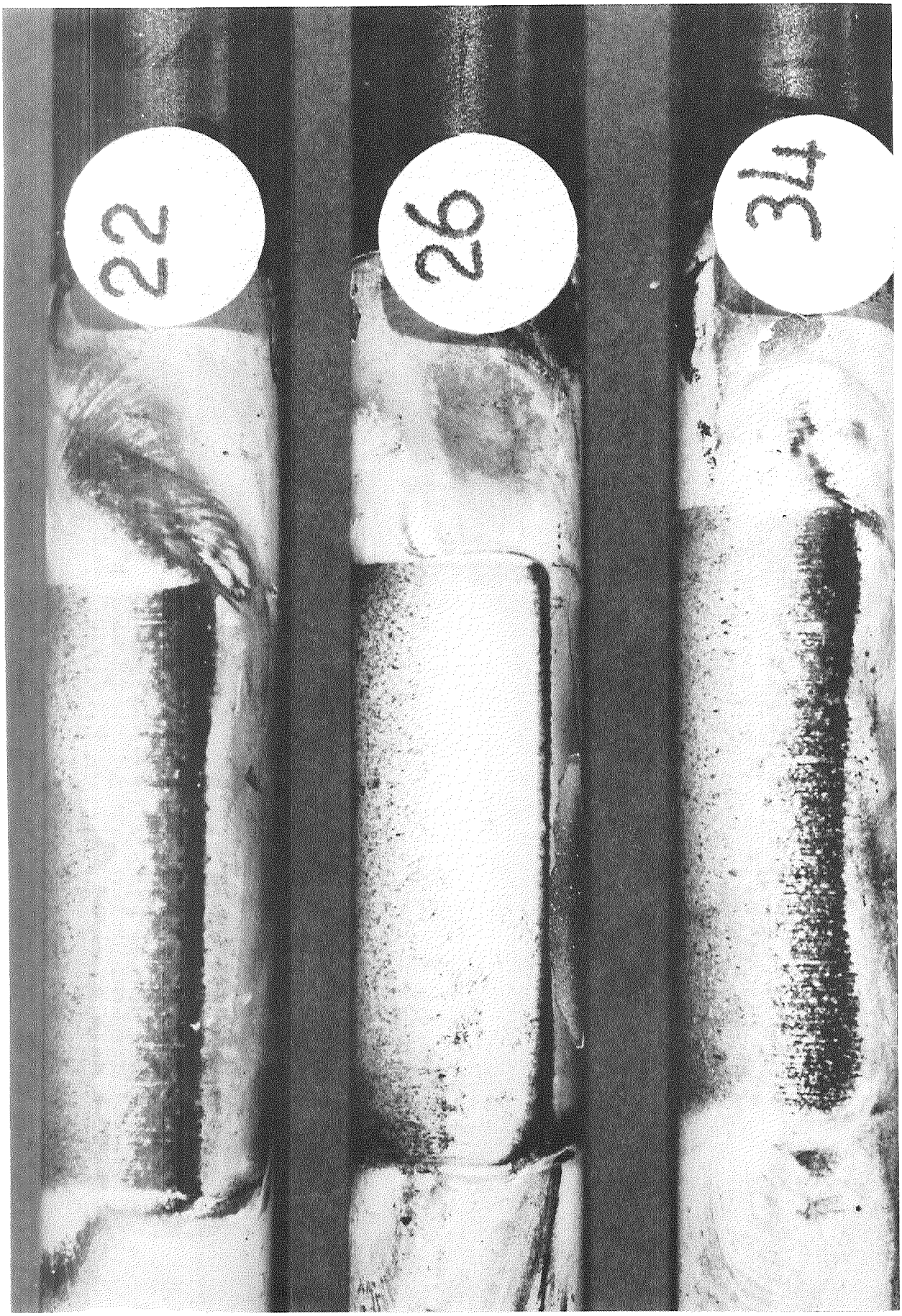

(b) Side; P_c = 302 psi

5AG15-9/25/69-C1G

(c) Rear: The Surfaces Away From The Injector. P_c = 302 psi

5AG15-9/25/69-C1I

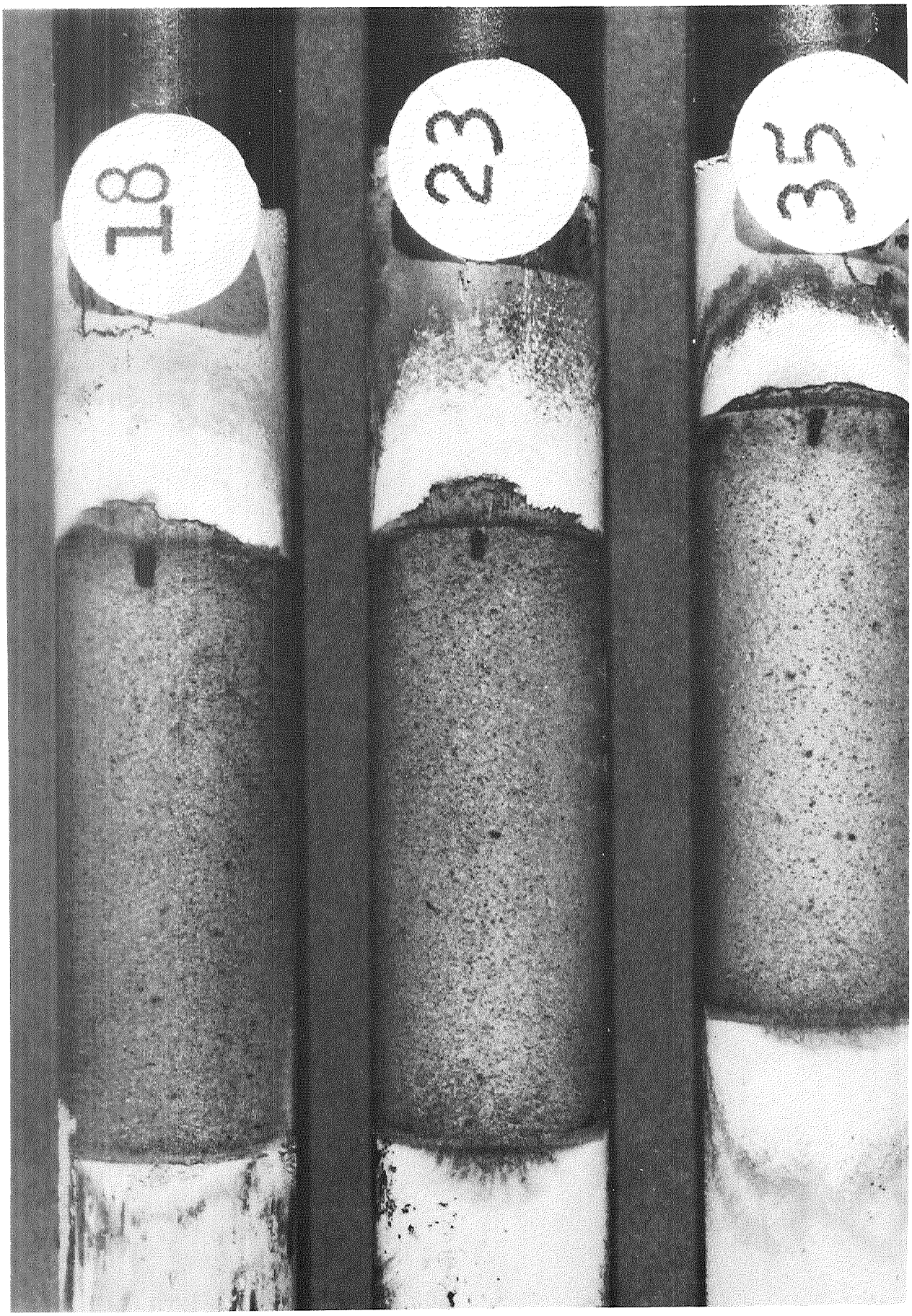

Figure 13. Coated-Tube Specimens After Rocket Engine Test at P_c = 442 psia.
(a) Front: The Surfaces Facing the Injector

5AG15-9/25/69-C1F

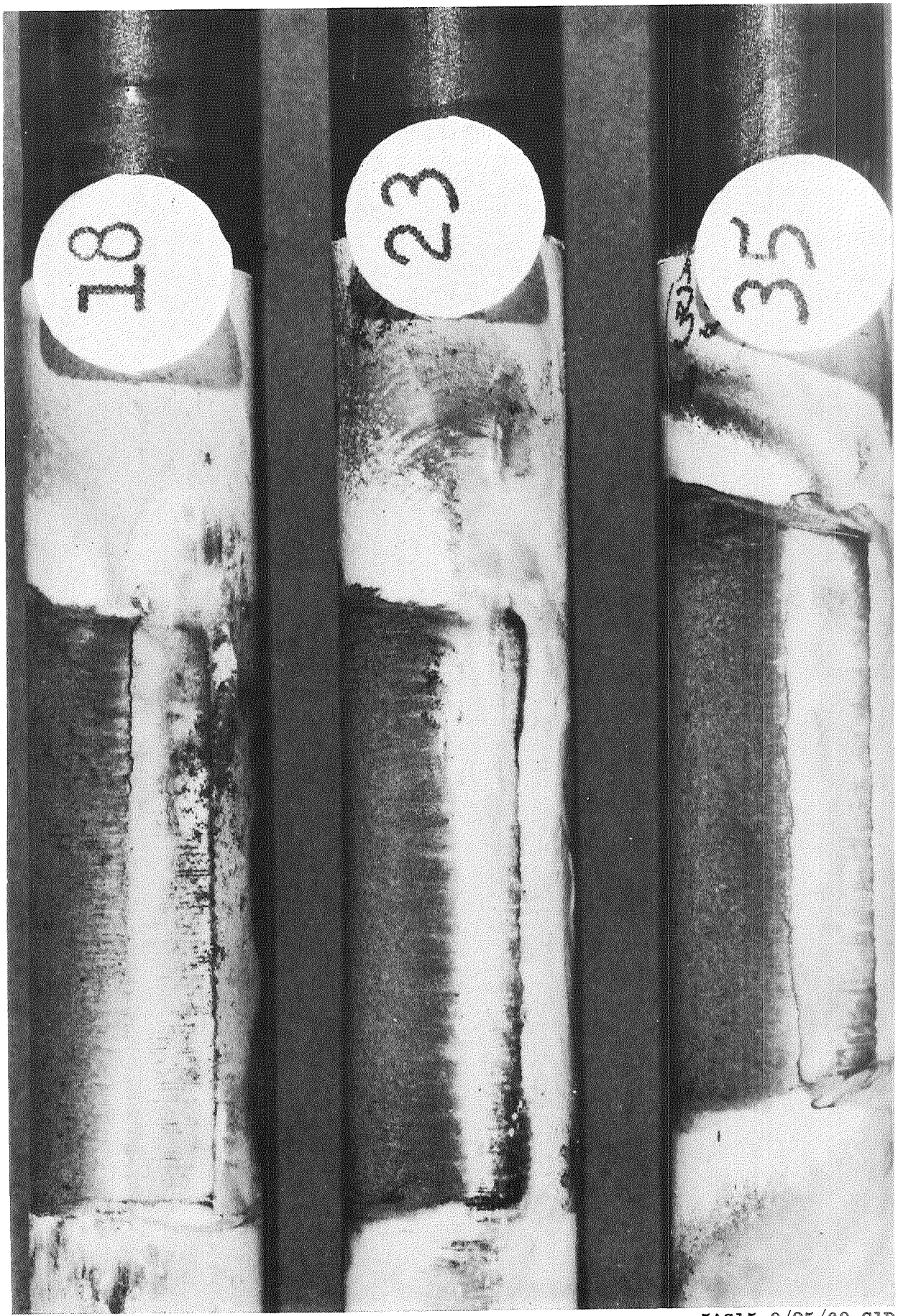

(b) Side: P_c = 442 psia

5AG15-9/25/69-C1D

(c) Rear: The Surfaces Away From the Injector. P_c = 442 psia.

5AG15-9/25/69-C1E

Figure 14. Coated-Tube Specimens After Rocket Engine Test at P_c = 575 psia.
(a) Front: The Surfaces Facing the Injector.

5AG15-9/25/69-C1C

(b) Side: P_c = 575 psia

5AG15-9/25/69-C1B

(c) Rear: The Surfaces Away From the Injector. P_c = 575 psia

5AG15-9/25/69-C1A

5AG15-9/22/69-C1A

Figures 15a, b, c. Specimens After the Checkout Test Firings at P_c = 302 psia. From Top to Bottom: An Uncoated Hastelloy-X Tube, Specimens 10 and 12 Coated with Slurry B45. Magnification X4-1/2.

(a) Front: The Surfaces Facing the Injector

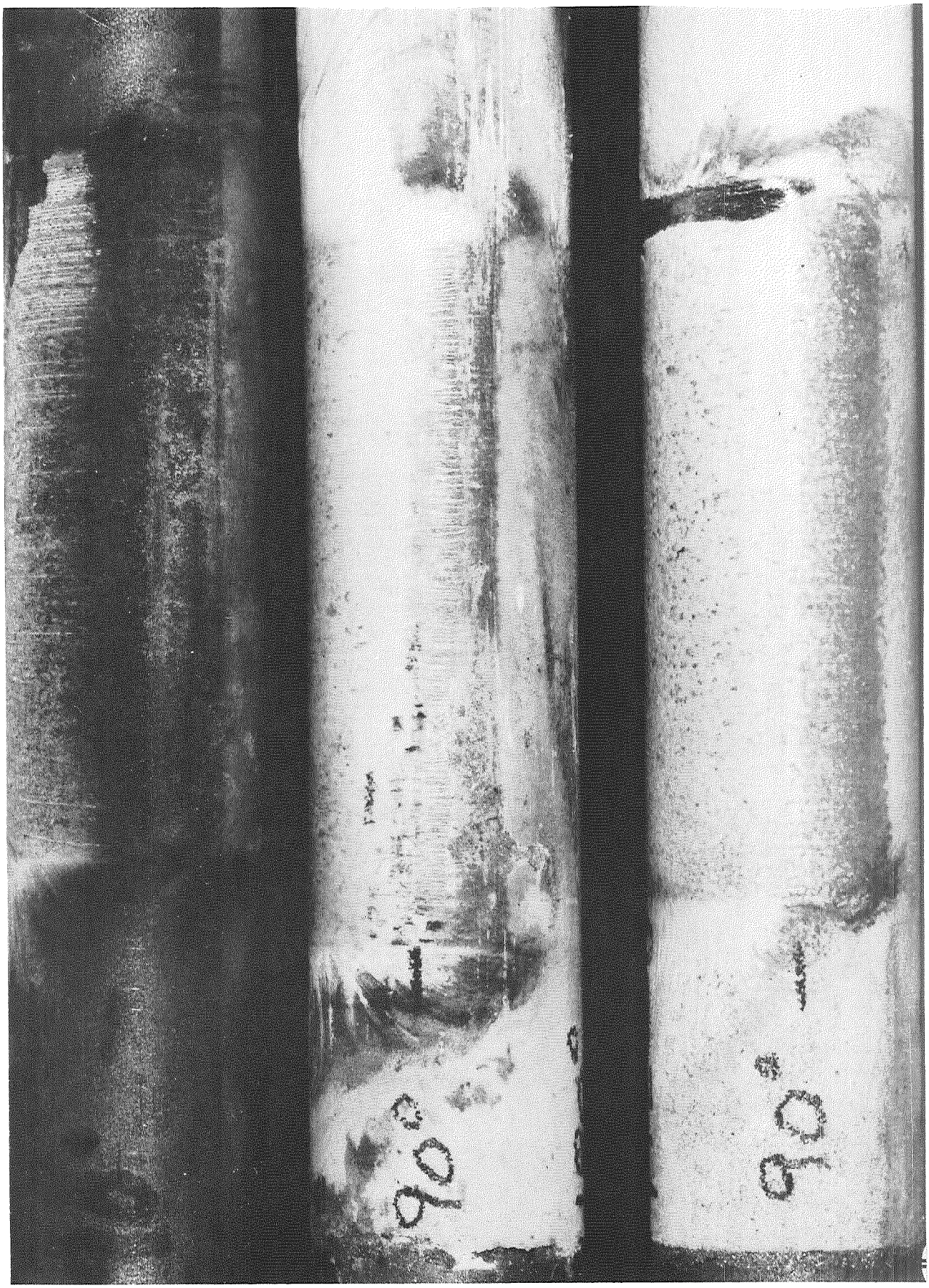

(b) Side: P_c = 302 psia

(c) Back: The Surface Facing Away From The Injector. P_c = 302 psia

5AG15-9/22/69-C1B

mechanical tensile stresses placed on the coating due to bowing of the tubes represent an unusually severe test condition.

Coating Microstructure.

General. Four sections of every specimen (except 25 and 28) were cut perpendicular to the tube axis and prepared for microscopic examination. Three sections were 1/4 inch apart starting 1/4 inch from the top of the one-inch zone that was exposed to the throat. An additional section was taken from the unexposed coated zone 1/4 inch above the top of the test zone. Only two usable sections could be cut from specimens 25 and 28 because they were so shortened after they were cut out of the throat fixture.

Coating Integrity. In general, integrity of the coating in the test zone was as good as that coating outside the test zone. Small portions of coating spalled when sectioned with the alumina cutoff wheel, and some zirconia grains pulled out during the grinding and polishing operations; but this occurred in Task II and in as-prepared specimens too. Thus, the general condition of the coating after engine testing was very good.

Coating Thickness. Coating thickness data obtained using a filar eye piece on the microscope is referred to as "true" thickness as compared to thickness data obtained using a micrometer or a nondestructive measurement instrument. True thicknesses were found to be slightly less than the nondestructively measured values. Thickness values for specimens averaged 1.7 to 3.3 mils with peak values near 4.0 mils (Table II) rather than that of the goal of 3.5 to 5.0 mils. The coating thickness around the tubes varied less than one mil in most specimens.

TABLE II

COATING THICKNESS DATA OF TUBE SPECIMENS

TESTED IN THE ROCKET ENGINE FIRINGS

Specimen	Nominal Chamber Pressure (psi)	Coating Condition	Coating Thickness (mils, Using the Dermitron); Degrees from Stagnation Point: 0	90	180	270	Avg	Coating Condition	Coating Thickness (mils, Using the Ceramographic Method); Degrees from Stagnation Point: 0	90	180	270	Avg
22	302	After[1]	2.5	1.4	1.7	3.9	2.4	Test[2]	2.8	1.9	2.0	2.7	2.4
		Before	2.7	1.6	2.0	3.2	2.4	Untested	2.9	1.5	1.6	2.8	2.2
		Net	-0.2	-0.2	-0.3	0.7	0.0	Net	-0.1	0.4	0.4	-0.1	0.2
26	302	After	2.7	2.2	3.9	3.4	3.3	Test	2.5	2.9	3.9	3.7	3.3
		Before	3.0	2.7	4.0	3.6	3.3	Untested	2.5	2.6	3.2	3.3	2.9
		Net	-0.3	-0.5	-0.1	-0.2	0.0	Net	0.0	0.3	0.7	0.4	0.4
34[3]	302	After	1.2	2.4	2.3	2.3	2.1	Test	2.4	1.5	2.1	1.9	2.0
		Before	2.4	2.7	2.5	2.3	2.5	Untested	2.0	--	1.5	2.2	1.9
		Net	-1.2	-0.3	-0.2	0.0	-0.4	Net	0.4	--	0.6	-0.3	0.1
23	442	After	2.2	2.6	2.8	2.2	2.5	Test	2.1	2.9	2.8	2.2	2.5
		Before	2.9	2.8	3.1	2.5	2.8	Untested	1.9	3.5	2.6	2.2	2.6
		Net	-0.7	-0.2	-0.3	-0.3	-0.3	Net	0.2	-0.6	0.2	0.0	-0.1
18	442	After	2.7	3.3	2.8	3.2	3.0	Test	2.9	3.0	3.4	3.9	3.1
		Before	3.0	3.0	3.0	3.1	3.0	Untested	2.2	2.2	3.0	3.0	2.6
		Net	-0.3	0.3	-0.2	0.1	0.0	Net	0.7	0.8	0.4	0.9	0.5

TABLE II

(Continued)

Specimen	Nominal Chamber Pressure (psi)	Coating Condition	Coating Thickness (mils, Using the Dermitron); Degrees from Stagnation Point: 0	90	180	270	Avg	Coating Condition	Coating Thickness (mils, Using the Ceramographic Method); Degrees from Stagnation Point: 0	90	180	270	Avg
35(3)	442	After	1.6	2.3	1.7	1.6	1.8	Test	1.5	2.4	1.7	1.6	1.9
		Before	--	--	--	--	--	Untested	1.5	2.3	2.2	1.6	1.9
		Net	--	--	--	--	--	Net	0.0	0.1	-0.5	0.0	0.0
25	575	After	2.0	2.4	2.1	2.7	2.3	Test	1.7	2.4	2.1	2.7	2.6
		Before	2.6	2.1	2.6	2.6	2.5	Untested	2.6	--	1.7	2.8	2.4
		Net	-0.4	0.3	-0.5	0.1	-0.2	Net	-0.9	--	0.4	-0.1	0.2
28	575	After	2.6	2.5	2.4	3.8	2.9	Test	1.9	2.5	2.4	3.8	2.7
		Before	3.6	2.5	2.3	3.1	2.9	Untested	2.2	2.0	2.3	3.0	2.4
		Net	-1.0	0.0	0.1	0.7	0.0	Net	-0.3	0.5	0.1	0.8	0.3
32(3)	575	After	1.9	--	1.7	1.8	1.8	Test	1.3	--	1.9	1.8	1.7
		Before	2.3	1.3	2.5	3.1	2.3	Untested	1.7	1.7	1.9	2.9	2.1
		Net	-0.4	--	-0.8	-1.3	-0.5	Net	-0.4	--	0.0	-1.1	-0.4
10	294							Test	1.9	3.1	3.0	2.9	2.7
								Untested	2.2	2.4	2.5	2.8	2.2
								Net	-0.3	0.7	0.5	0.1	0.5

TABLE II

(Continued)

Specimen	Nominal Chamber Pressure (psi)	Coating Condition	Coating Thickness (mils, Using the Dermitron); Degrees from Stagnation Point: 0	90	180	270	Avg	Coating Condition	Coating Thickness (mils, Using the Ceramographic Method); Degrees from Stagnation Point: 0	90	180	270	Avg
12	294							Test	1.9	1.6	1.5	--	1.7
								Untested	1.7	1.6	--	--	1.7
								Net	0.2	0.0	--	--	0.0

(1) After: Measurement of coating thickness was made after testing.

Before: Measurement of coating thickness was made before testing.

Net: Net gain or loss in coating thickness.

(2) Test: The destructive measurement was made 1/4 inch below the top of the portion of specimen exposed to the test environment.

Untested: The destructive measurement was made 1/4 inch above, and outside, the portion of specimen exposed to the test environment. This measurement is indicative of coating thickness in the test area before testing.

Net: Net gain or loss of coating thickness.

(3) These speciments were coated with slurry composition B44; all other specimens were coated with composition B45.

Erosion. Although erosion must have occurred because the coating on the surface melted and flowed, appreciable erosion was not indicated by thickness measurements. Thickness values of the coating before and after the test firing, which were obtained nondestructively with the Dermitron, are listed in the wide center column of Table II. Average indicated net loss of coating thickness was nominal, 0.0, 0.0, 0.4, 0.3, 0.0, 0.2, 0.0, and 0.5 mil. Thickness data listed in the right-hand column of Table II were obtained on mounted sections by a standard ceramographic method. Obviously, specimens could not be destroyed before testing, so the "before testing" data were obtained after testing but from a coated area near, but outside of, the test zone. Coating thickness in the untested zone should be close to that in the test zone before testing because nonuniformity of the thickness should be small over the axial distance of only 1/2 inch that separated the two measurement locations. These data indicate, on the average, an increase in coating thickness from the untested to the tested region, and that the highest loss in thickness at the stagnation point for a single specimen was only 0.3 mil. These data, therefore, indicate that erosion was essentially nil.

Fusion. The most apparent microstructural change in the coating was the fusion and/or sintering of the zirconia grains at the hot-side surface. Grains nearest the surface and in the highest heat flux areas actually melted and flowed. The flow lines are apparent in Figs. 12c, 13c, and 14c. Motion picture films of the test showed that this flow lasted only a fraction of a second before equilibrium was obtained. Figure 16 shows two photomicrographs of the coating in a mounted section that was polished to the middle of a flow line. The coated area in the top photomicrograph was located 100 degrees from the stagnation point,

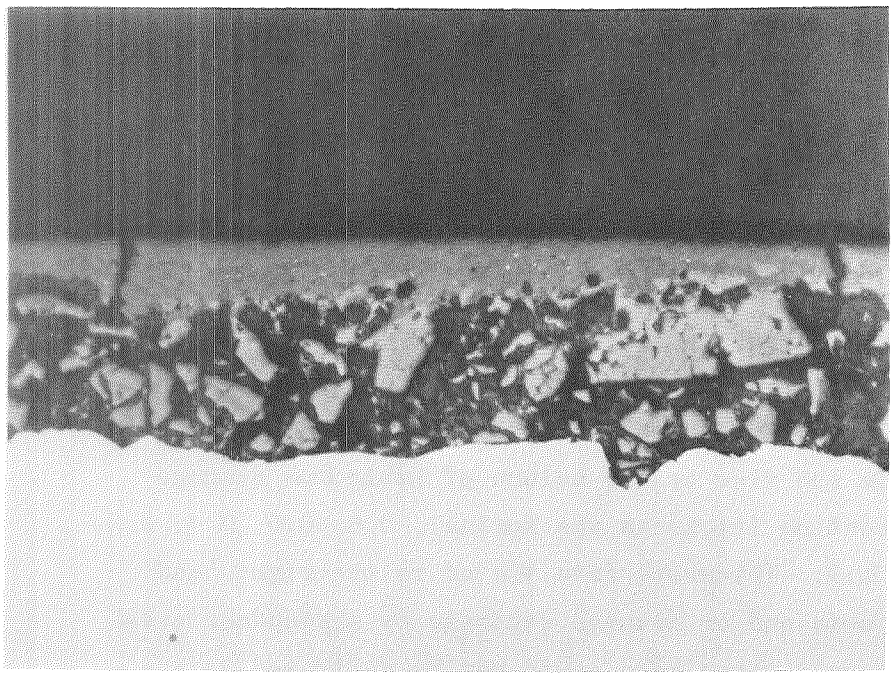

Mounting Material

Specimen 25:

Test Zone;
100° from stagnation point

Hastelloy-X

740

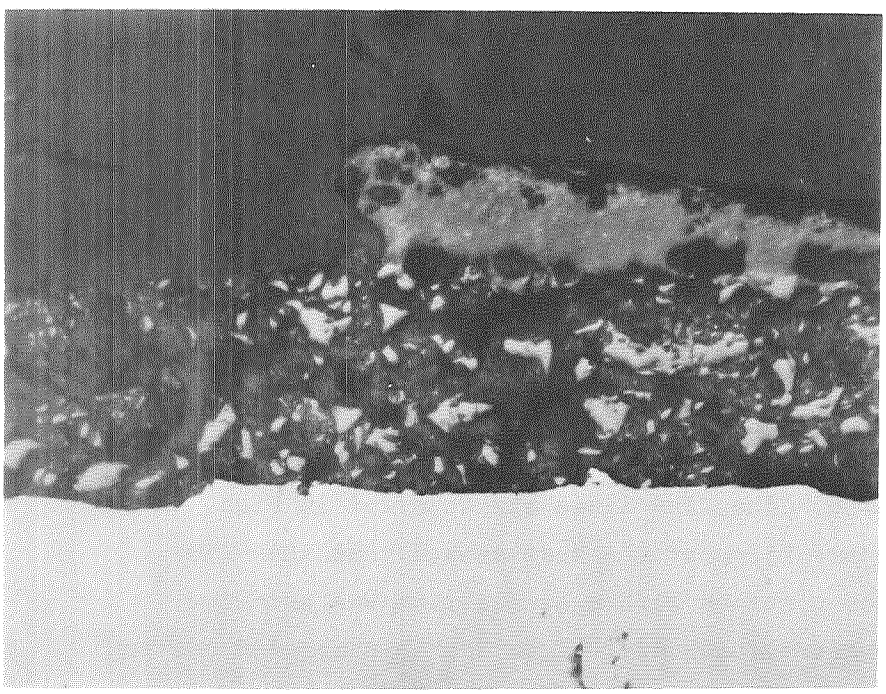

Mounting Material

Specimen 28:

Test Zone;
135° from stagnation point

Hastelloy-X

744

Figure 16. Photomicrographs of Sections Cutting Through The Coating Flow Lines. (Magnification X400)

while the one at the bottom was located about 135 degrees from the stagnation point. The photomicrograph at the bottom shows the end of the flow line where separation of the combustion gases occurred. Fusion was observed, thus, from the stagnation point to 135 degrees to either side. Relating degree and depth of fusion to heat flux at any point around the circumference of the specimen, therefore, is somewhat difficult because, depending on coating thickness and the heat flux through the coating, fusion and/or sintering may not have wholly originated at that point. The fused surface, or a portion of it, could have been transported there from upstream. Note that the coatings under the flow lines in Fig. 16 show no effect of excess heating. For the majority of specimens, differentiating between zirconia grains that fused in place and those that were transported to that point in the molten state was not so easy as Fig. 16 suggests.

The highest density of the heat-affected depth of coating generally was observed at the stagnation point, and in a few specimens, at about plus and minus 45 degrees from the stagnation point. Estimation of density was not precise, however, due to nonuniformity in the microstructure, pullout of grains during polishing operations, and the fact that it was not always possible to determine whether the section was cut through or alongside a flow line of molten coating.

Maximum depth to which the effects of heat were observed varied from 30 to 100 percent of total thickness, and it increased with chamber pressure. The largest depth of heat-affected coating was observed within plus and minus 45 degrees from the stagnation point. Figure 17 shows photomicrographs of two specimens that have been affected considerably by the high temperature.

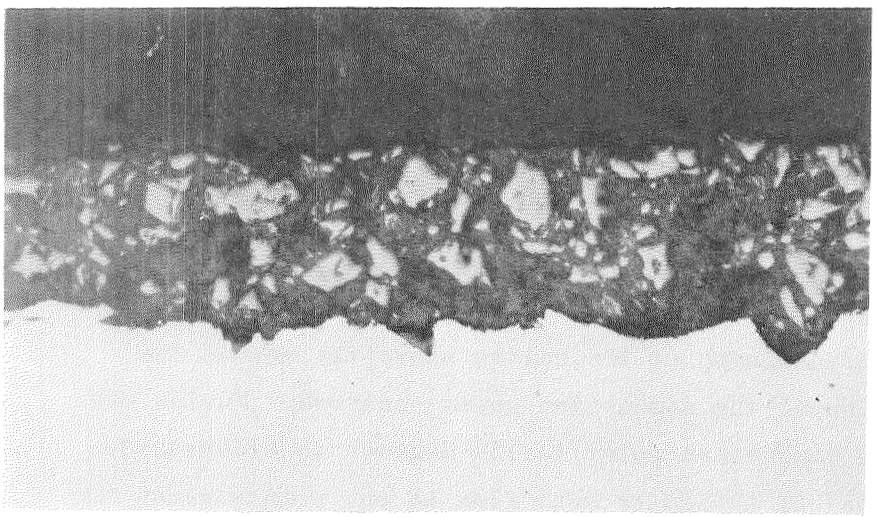

Mounting Material

Typical microstructure in a low heat flux location

Hastelloy-X

741

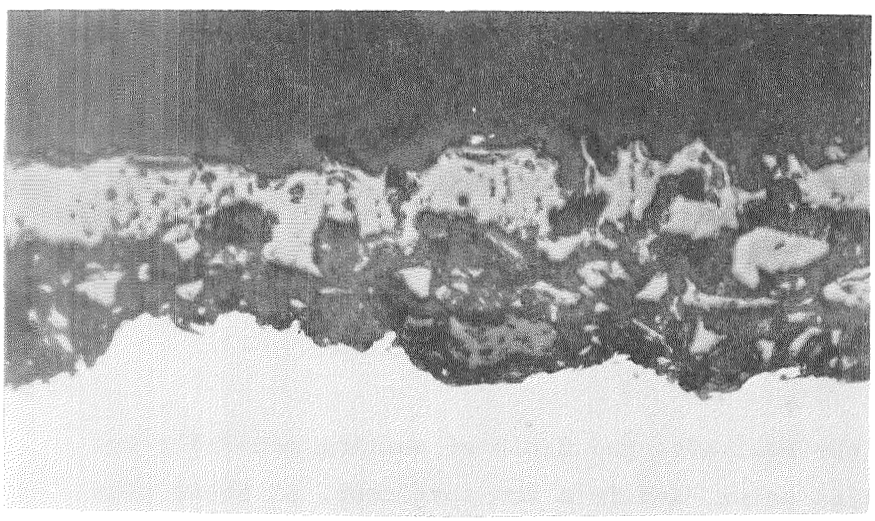

Mounting Material

Specimen 34

Test Zone;
0° from stagnation point

Hastelloy-X

735

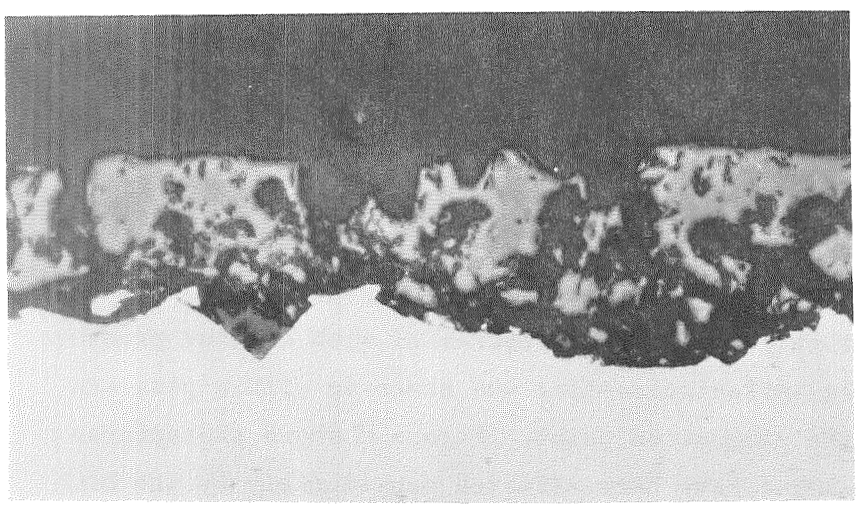

Mounting Material

Specimen 35:

Test Zone;
30° from stagnation point

Hastelloy-X

738

Figure 17. Microstructure of Coated Specimens Tested in the Rocket Engine Comparing Effects of Temperature. Magnification X400.

Comparable microstructures are found in Reference 1, pp. 81 and 82, wherein the coated specimens attained an optical pyrometer temperature of more than 4400 F in arc-plasma jet tests. Based on comparable tests in the arc-plasma jet, then, the evidence is that surface temperatures of the coated specimens tested in the rocket engine reached 4400 F.

Influence of Phosphate Content. Clear-cut comparison of test specimens coated with B44 and B45 compositions, 0.5 and 1.1 parts phosphate binder solution per 10 parts by weight zirconia, was not possible. Test conditions were different for the two types of test coating formulations because coating thickness of B44-coated specimens was thinner than that of B45-coated specimens. One interesting but uninterpretable observation was made, however. Specimens coated with B44 slurry fused more but flowed less than specimens coated with B45 slurry in the 302 and 442 psia chamber pressure runs. B44-coated specimens behaved as follows: specimen 34, which was tested at 300 psia, fused to a maximum depth of 40 percent of total thickness while 35, which was tested at 450 psia, fused to a maximum depth of 90 percent. Yet neither coating flowed appreciably compared to B45-coated specimens. All coatings flowed noticeably in the 600 psia run.

Summary

Although these tests did not resolve optimum coating thickness or phosphate content, they did demonstrate that both slurry formulations afforded considerable, up to 40%, heat reduction, and that they are capable of surviving the reference rocket engine environment.

ROCKET MOTOR TEST RESULTS: TUBULAR-WALL, TWO-DIMENSIONAL THROAT SECTION

A limited series of rocket motor firings was made using the single tubular-wall specimen coated with phosphate-bonded zirconia. The Hastelloy-X tubes which formed one wall of a two-dimensional throat segment were internally cooled with water. The tests, runs 90, 91, and 92 were conducted at mixture ratios of 7.0, 6.2, and 6.0 and at chamber pressures of 244, 366, and 506 psia, respectively. Coating thickness averaged 2.9 mils. Pertinent data for the engine environment and the heat transfer through the coated and uncoated walls are listed in Table III.

The reduction of average heat flux at 244, 366, and 506 psia is 30, 40, and 46 percent, respectively. A complete discussion of the heat transfer results and assumptions made for correction of the heat flux may be found in Appendix A. Total data correlation was not obtained from the data of the calorimeter due in part to known problems with instrumentation. Therefore, it was not possible to make a direct assessment of local heat transfer reduction by the coating. If the throat heat transfer is about 1.6 times the average, the maximum flux through the coating in the throat region was about 13 Btu/in^2-sec. It can be concluded that increasing the coating thickness to 3.5 mils would result in the design goal of thermal performance; that is a heat flux reduction from 50 to 20 Btu/in^2-sec.

Visual Evaluation

Before Test Firing. Photographs of the tubular wall before and after the coating was applied are shown in Figs. 5b and 18. The coating appeared uniform but the surface texture was slightly rougher than desirable. Loca-

TABLE III *

SUMMARY OF ROCKET MOTOR TESTS ON TUBULAR WALL

Run Number	Mixture Ratio	Chamber Pressure (psia)	Duration (sec)	Characteristic Velocity Efficiency (η_{c*})	Average Integrated Heat Flux for the Coldwall Calorimeter (Btu/in^2 sec)	Corrected Average Heat Flux for the Coated Tube Wall (Btu/in^2 sec)	Reduction of Heat Flux %
90	7.0	244	20	99.4	8.5	5.9	30
91	6.2	366	20	98.1	12.0	7.1	40
92	6.0	506	20	99.4	15.2	8.4	46

* See Table A-2 for detailed heat transfer data.

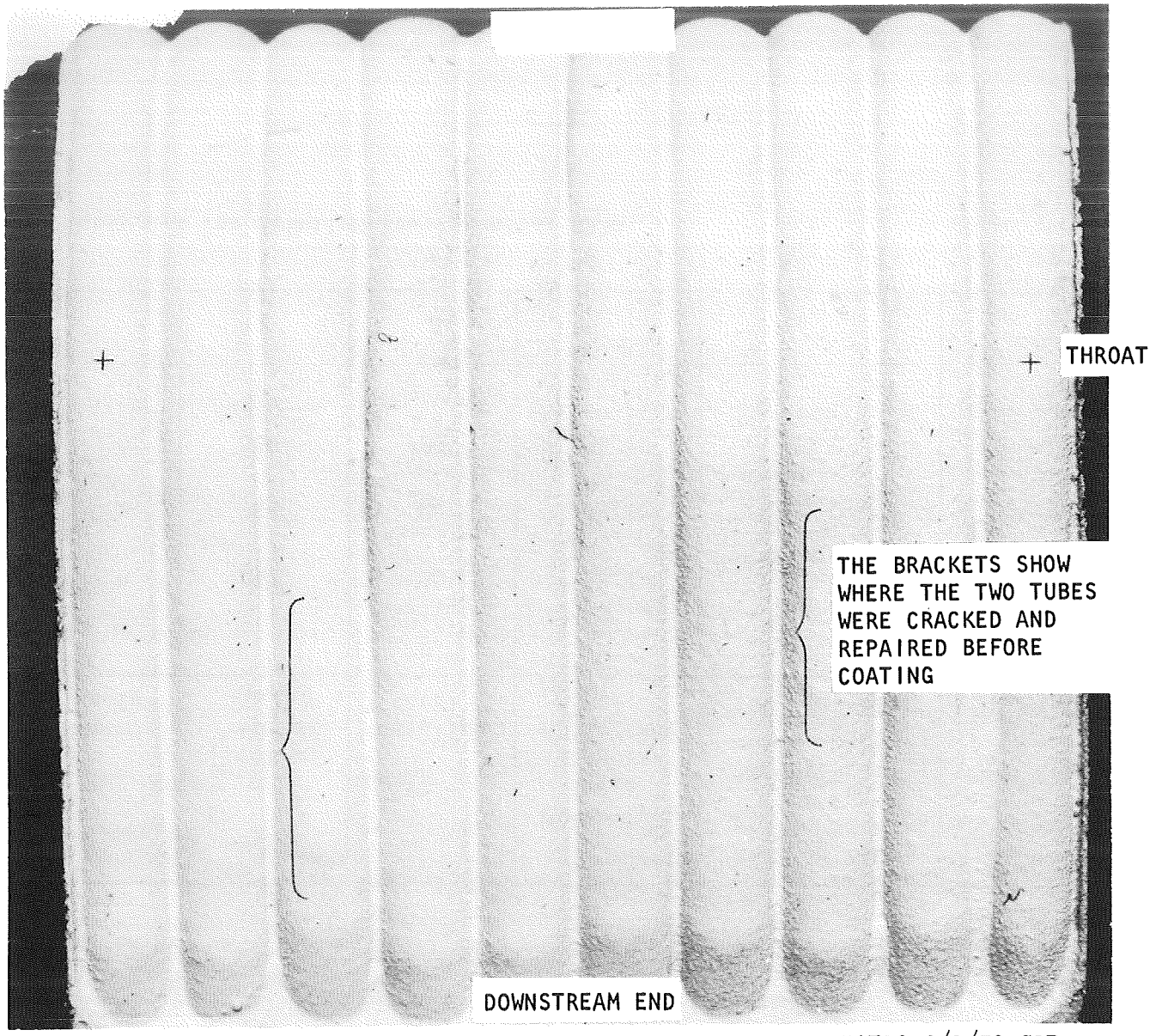

Figure 18. Top View of Tube Wall in the Coated Condition (Mag X3.3).

tion of the two repaired areas, indicated in Fig. 18, were not apparent after the coating was applied, nor for that matter, after the bare tube was grit-blasted.

Coating thicknesses at the throat on the two-side tubes were 3.2 and 2.3 mils (see Fig. 18). These values were obtained with a four-inch micrometer by measuring the thickness of the entire body before and after the coating was applied. Due to irregularities on the back surface, these measurements may not be very accurate. Coating thickness was also measured on the glass slide positioned adjacent to the tubular wall during the coating spraying operation. Coating thickness at locations about every 3/8-inch and starting at the upstream end was 3.3, 3.5, 2.5, 3.0, and 2.6 mils on one side and 3.3, 3.0, 2.5, 3.0, and 2.7 mils on the other side. Average value for a thickness measurement is 2.9 mils.

The coating unavoidably was subjected to some abuse while the tubular wall block assembly was inserted into the rest of the throat segment. Most significantly, two pieces of coating were chipped from the tubes in the most crucial throat area (Fig. 19a). A steel block was placed in the throat gap while the tubular wall block assembly was pushed in place. The side clearance was more than anticipated, enough so that the tubular wall assembly block slipped in easily and hit the steel positioning block hard enough to chip the coating in at least two locations. Of less consequence, grease or dirt was smeared on the coating. Some of the smears are visible in Fig. 19a.

After the First Firing. Integrity of the coating was visibly unaffected by the first 20-second run at a chamber pressure of 244 psia. The coating was hard, and no cracks or spotted areas were visible. (Hardness was evaluated by scratching with a fingernail.) The coating was slightly discolored pale gray or blue-gray in some areas (Fig. 19b). The size of the chipped areas present before testing in the throat did not change. This was very significant because it seemed likely that the shear forces from the combustion gases could have lifted the coating off, peeled it back and, thus, caused spalling. The fact that the coating stayed on indicates that it was tenaciously bonded to the Hastelloy-X substrate.

After the Second Firing. Integrity of the coating, in general, remained very good after the second firing (Fig. 19c), this time at a chamber pressure of 366 psia for 20 seconds. No cracks were observed and the coating was still hard.

A strip of coating along the crown of the tube on the left side (looking into the injector) did spall, however. This is surprising because environmental conditions on the coating at this location are the least severe compared to any other axial position. Logical explanations are that: (1) the thermal stresses were inordinately high here due to the constraint of the copper wall and to differences in cooling caused by the proximity of the copper walls, or (2) the coating was damaged (but not visibly) during the assembly operation. The larger of the two areas that were chipped before firing increased in size about 1 mm. A tenuous flake of coating at the edge of the chipped area spalled.

After the Third Firing. Integrity of the coating, in general, remained very good after the third and final firing, 20 seconds duration at 506 psia. Over the major portion of the coating, that is excluding the periphery of the coated area, the coating appeared in good condition (Figs. 19d and 20): it was more discolored, some areas in the braze fillets appeared thinner, and a few very small pieces of coating spalled in the throat; but on the other hand, the original chipped areas did not get larger and no cracks or weakened areas were observed in the coating. Some spalling did occur, however. It occurred: (1) on the crown of the tube on the left side (Fig. 20), (2) in the rear over the braze-filled areas (Fig. 20), and (3) in the front where the coating was shielded, but not protected, from the combustion gases (Fig. 21).

These areas where the coating spalled were atypical and results must be viewed in this light. As stated above, the coating on the left side tube crown could have been damaged before testing or it could have been subjected to extra severe stress conditions. The coating that spalled in the downstream areas was applied over large braze fillets. This suggests that failure was due to a mis-match in properties between the braze alloy and coating. The coating, up to this time, had never been tested on any substrate but Hastelloy-X except for the small coated braze fillets evaluated in the arc-plasma jet test. Thus, the fact that the coating spalled to some degree in this zone was disappointing, but it was not surprising.

The coated area in the upstream end (Fig. 21) was subjected to unknown, and probably very severe, test conditions. This area was mated against

the face of the combustor. A recessed area had been milled in this face so that the protruding coated tubes would not be smashed when the throat insert was bolted to the combustor (refer to Fig. 8). Thus, there was an opening of unknown dimensions between the combustor face and the tubular wall. Hot combustion gases flowed into this open slot, but since the environmental conditions are unknown, the heat transfer conditions cannot be evaluated. Damage to the coating in this zone could have resulted from the milled slot being too small such that when the tube crowns expanded due to heating from the combustion gases, they pushed into the face of the combustor, crushing the coating.

Repaired Tubes. The coating was unaffected by the series of three tests where it was applied over the braze-repaired tubes (see Figs. 18 and 20). This demonstrated the possibility of extending the life of the thrust chambers by repairing and recoating certain areas, even after some tubes have failed.

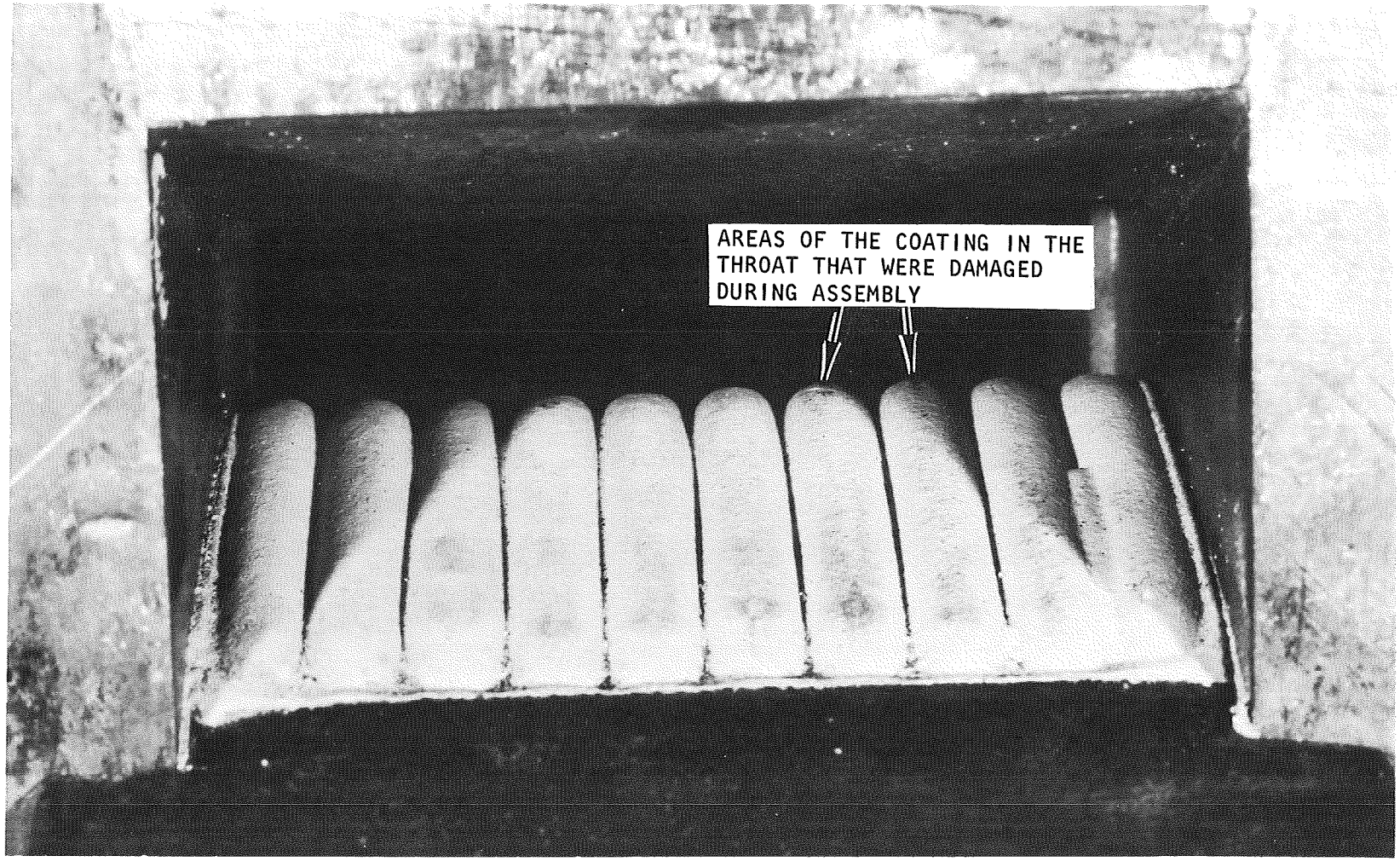

5AA36-10/30/70-S1C

Figure 19a. Tubular Wall Mounted in the Throat Segment (Looking in the Combustor Toward the Injector) Before Test Firing.

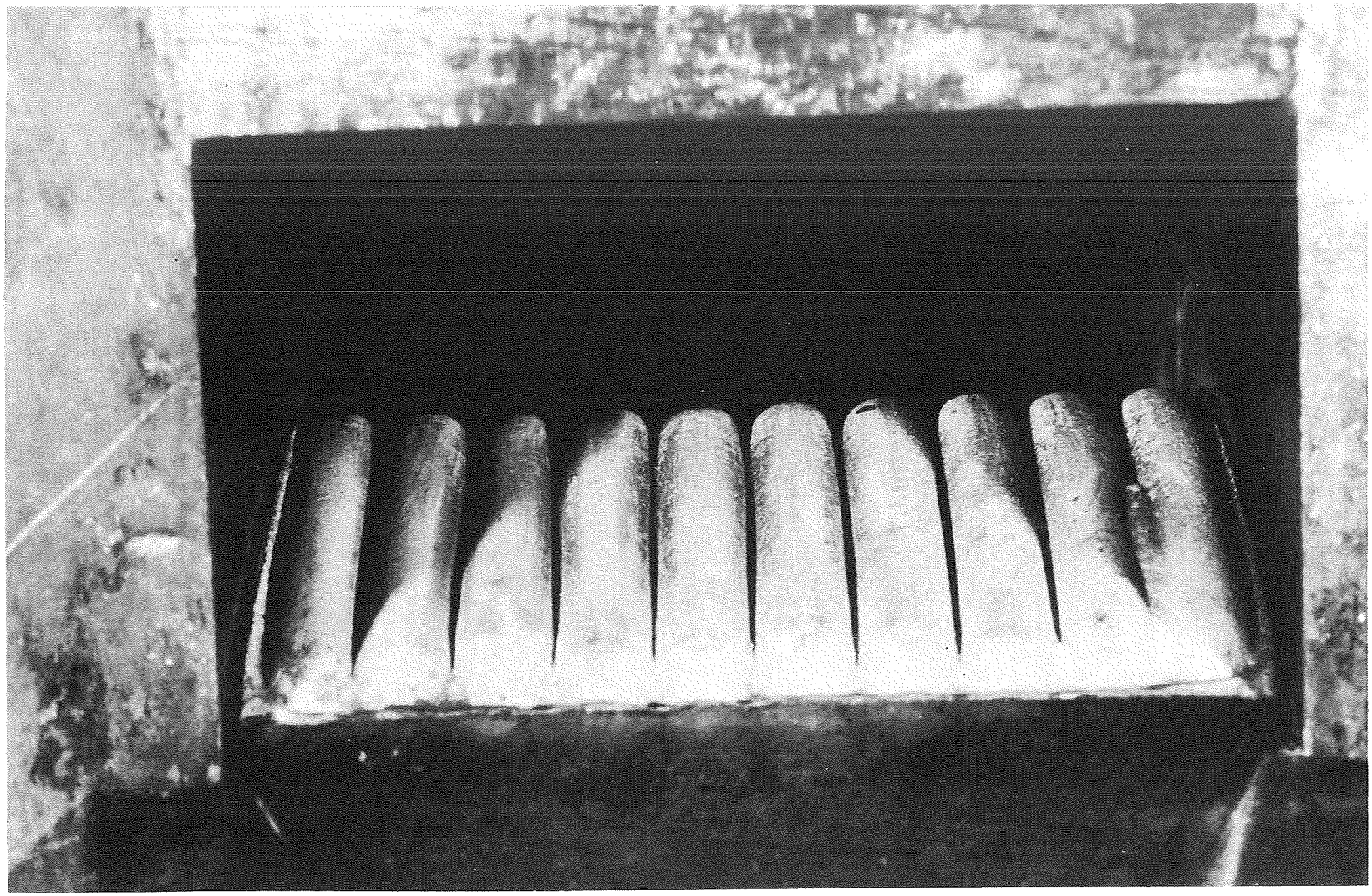

5AA36-10/30/70-S1D

Figure 19b. Condition of the Coating After Firing for 20 Seconds at 244 psia Chamber Pressure

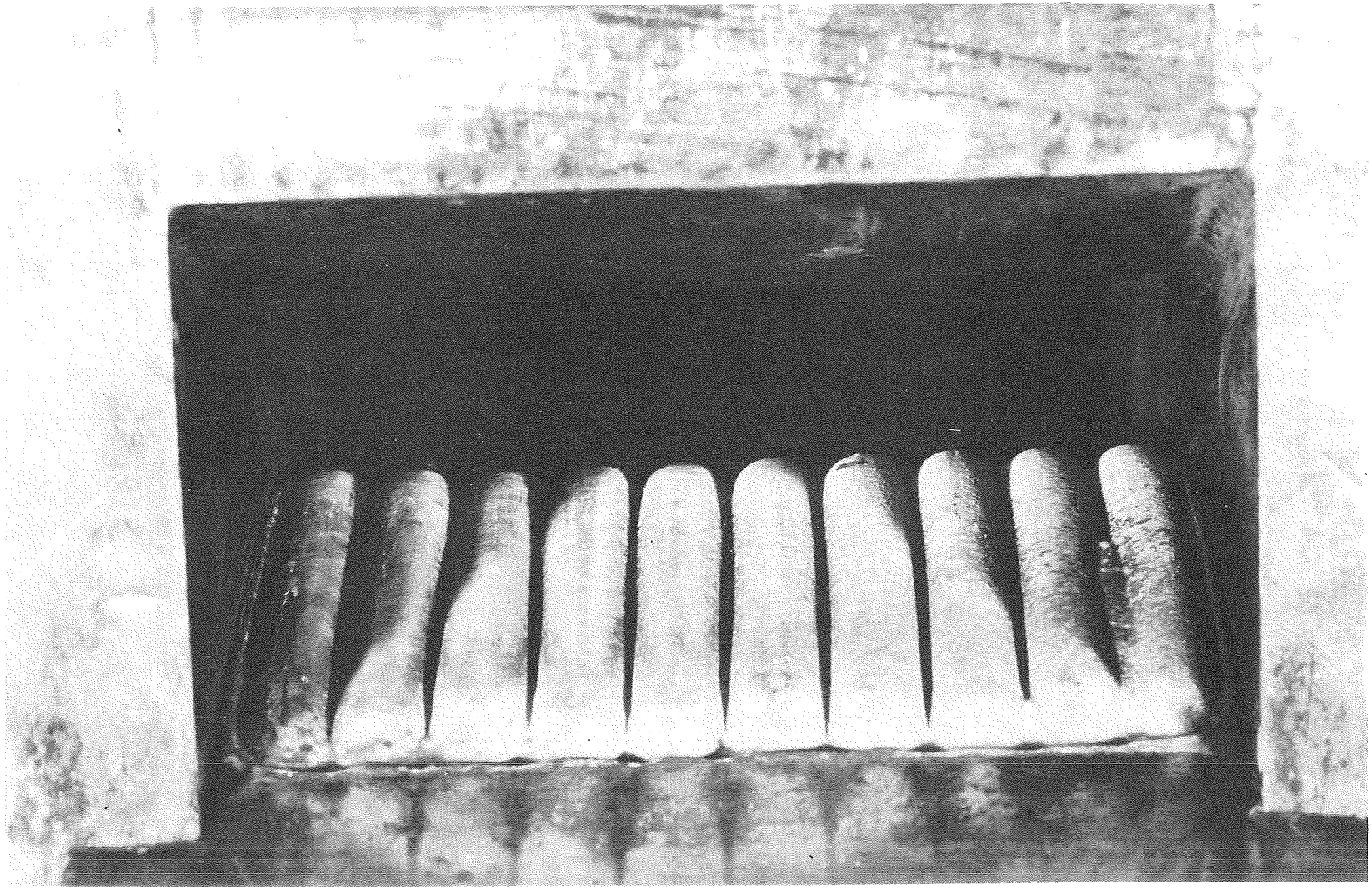

5AA36-10/30/70-S1A

Figure 19c. Condition of the Coating After Firing for an Additional 20 Seconds at 366 psia Chamber Pressure

5AA36-10/30/70-S1B

Figure 19d. Condition of the Coating After Firing an Additional 20 Seconds at 506 psia Chamber Pressure

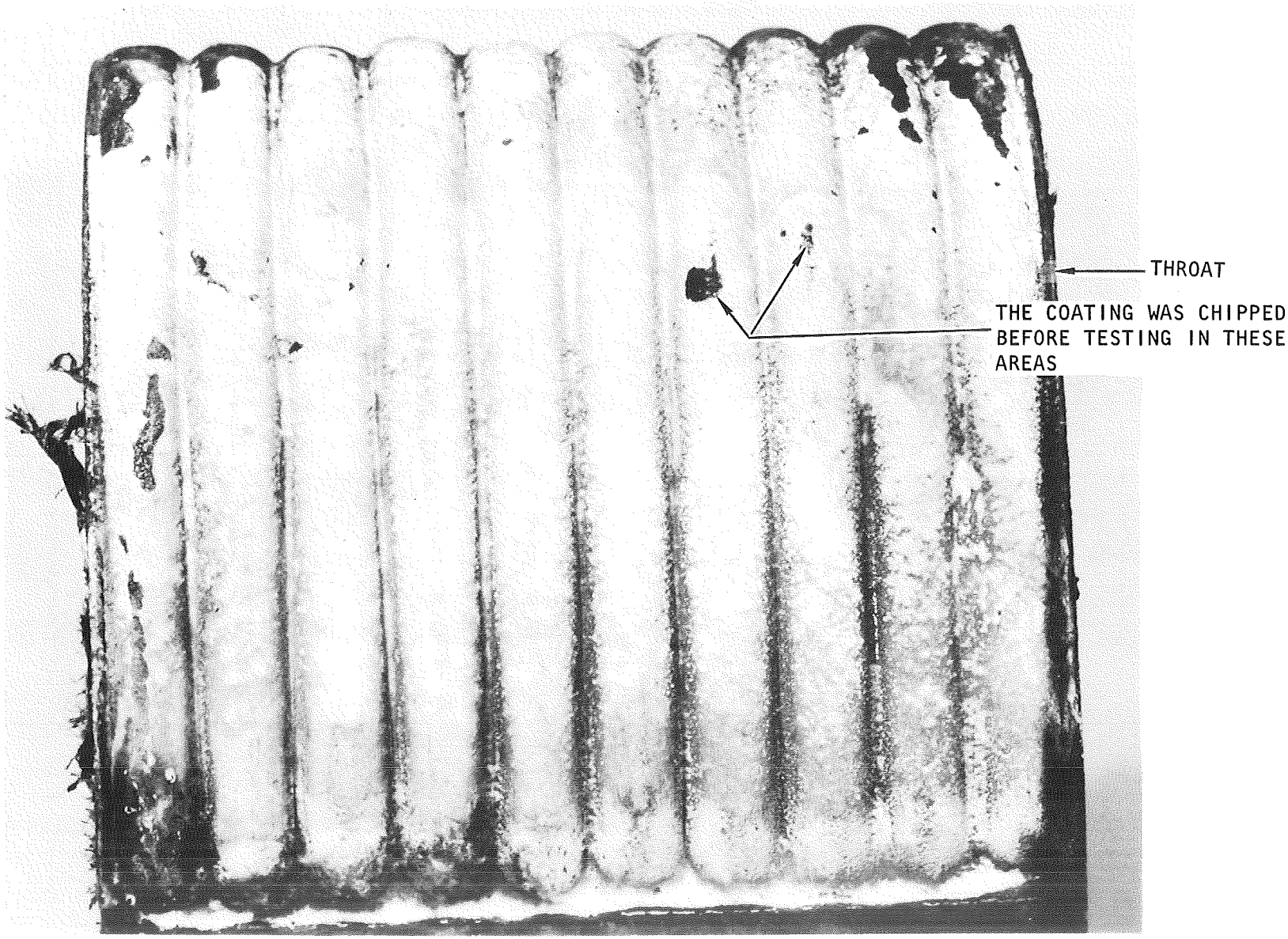

5AA36-10/30/70-S1E

Figure 20. Top View of the Coated Tube Wall After the Three Test Firings

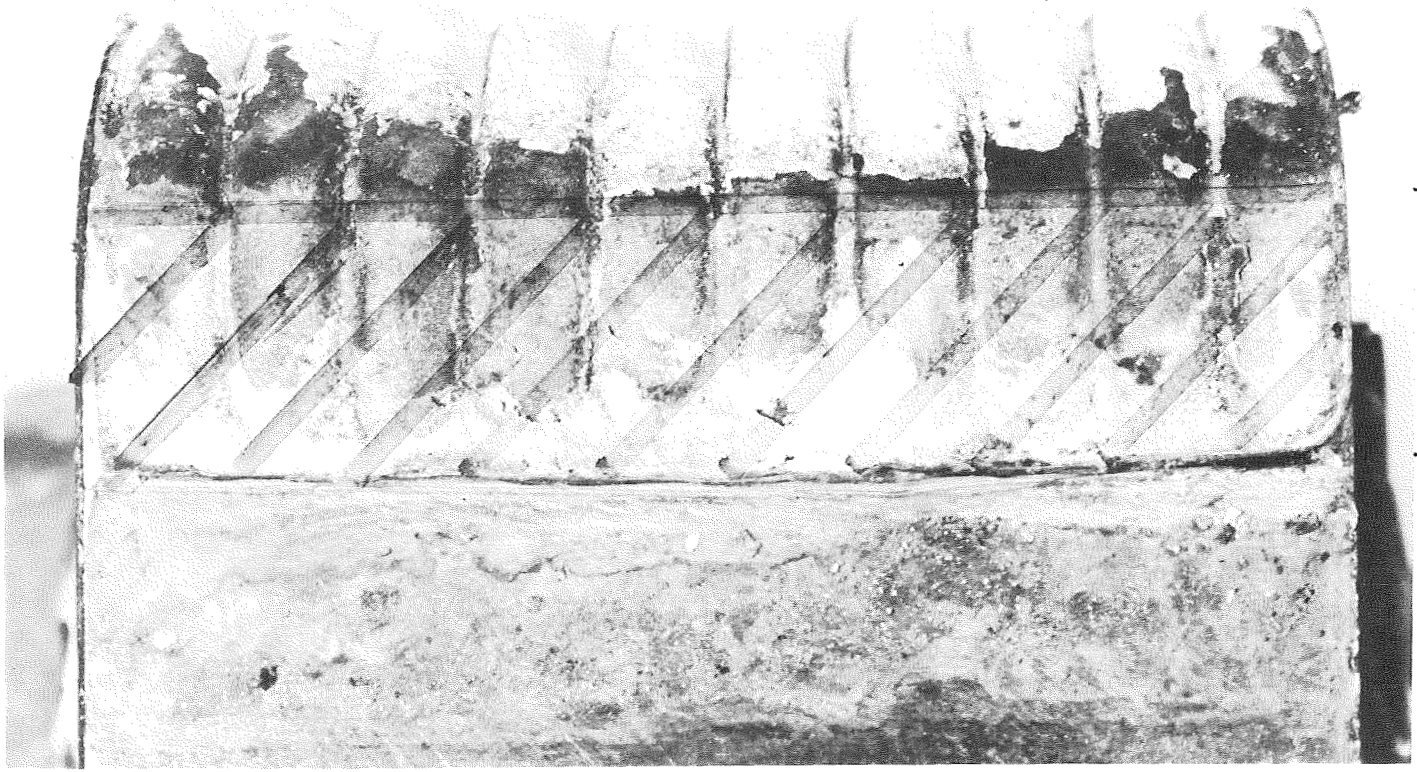

5AA36-10/30/70-S1F

Figure 21. Front View of the Coated Tube Wall After the Three Test Firings

CONCLUSIONS AND RECOMMENDATIONS

A program was concluded in which a heat-barrier coating for Hastelloy-X tubes was developed and tested under a variety of rocket engine conditions. Although several coating failures were noted, the results were generally very encouraging. In each case, the heat flux was reduced approximately as expected, depending upon the coating thickness and chamber pressure. The tenacity of the coating was shown to be very good even under conditions when the surface of the coating was melted and thermal stresses were very high. Failures were noted when the coating was placed in tension, hit with hammer-like blows, or were subjected to compressive crushing between metallic parts. Some of these failures are not likely to be avoided by any coating system, while other failures could have been avoided by redesign of test hardware.

Three general objectives need to be accomplished before the phosphate-bonded coating system can be applied to a large, full-scale thrust chamber with assurance of durability and a high confidence that the coating will have optimum properties. They are to 1) perform additional motor tests to better establish durability and usefulness, 2) further improve properties, and thus the reliability of the coating system, and 3) develop coating application processes for applying controlled thicknesses to large, complexly shaped thrust chambers.

REFERENCES

1. Carpenter, H. W., "Protective Coating System for a Regeneratively Cooled Thrust Chamber," Tasks I and II, Final Report, NASA CR-72569, February 1969.

2. Bartz, D. R., "A Simple Equation for Rapid Estimation of Rocket Nozzle Heat Transfer Coefficients," Jet Propulsion, 27, 1, p. 49, January 1957.

APPENDIX A - HEAT TRANSFER ANALYSES AND RESULTS

INDIVIDUAL TUBES

Throat-Tube Heat-Transfer Analysis

One of the primary objectives of the rocket motor firings was to determine the extent of heat flux reduction given by the phosphate-bonded zirconia coating. This heat flux reduction aspect of the coating program is given in this section of the report. Because the nature of the motor firings was not fundamentally heat transfer oriented, maximum use has been made of heat transfer results on previous programs. Specifically, the use of throat tubes as a test vehicle appeared to have several advantages early in the program and Talmor's data (Ref. A-1 and A-2) was used extensively.

The steady-state local heat transfer to a coated tube exposed to a rapidly accelerating external gas flow and an internal coolant flow can be expressed by (see Nomenclature List at end of this Appendix):

$$Q(\alpha) = h(\alpha)\ A_3\ (T_{aw} - T_{wg}) = \frac{T_{wg} - T_{wc}}{R_c} \qquad (1)$$

where: $R_c = \dfrac{\ln\ (r_3/r_2)}{2\pi\ k_c\ L_c}$ = thermal resistance of the coating.

Also,

$$Q(\alpha) = h_1\ A_1\ (T_{w1} - T_b\ ) = \frac{T_{wc} - T_{w1}}{R_H} \qquad (2)$$

where: $R_H = \dfrac{\ln\ (r_2/r_1)}{2\pi\ K_H\ L_H}$ = thermal resistance of the metal tube.

Combining equations (1) and (2), the local heat transfer may be expressed as the ratio of the overall temperature difference to the sum of the thermal resistances, or:

$$Q(\alpha) = \frac{A_3 \left(T_{aw} - T_b\right)}{\frac{1}{h_g(\alpha)} + A_3 R_c + A_3 R_H + \frac{A_3}{A_1 h_1}} \tag{3}$$

Integration around the tube circumference (α = 0 to 360°) gives the total heat flux.

Adiabatic Wall Temperature. The adiabatic wall temperature is related to the combustion-gas total temperature by,

$$T_{aw} = T_o \frac{1 + R_T \frac{\gamma-1}{2} M_\infty{}^2}{1 + \frac{\gamma-1}{2} M_\infty{}^2} \tag{4}$$

For turbulent boundary layers, the recovery factor, R_T, can be approximated by the relation:

$$R_T \sim Pr^{1/3} ; \tag{5}$$

thus,

$$T_{aw} = T_o \frac{1 + Pr^{1/3} \frac{\gamma-1}{2} M_\infty{}^2}{1 + \frac{\gamma-1}{2} M_\infty{}^2} \tag{6}$$

The bulk combustion-gas stagnation temperature is obtained from the theoretical combustion temperature corrected for the actual combustion efficiency:

$$T_o = T_{o_{theo}} (\eta_{c*})^2 \tag{7}$$

Gas Side Heat Transfer Coefficient. The local gas-side heat transfer coefficient around the tube was determined from the experimental and analytical work of E. Talmor (Refs. A-1 and A-2) who used extensive pressure and temperature measurements. The circumferential gas-side heat-transfer coefficient profile is shown in Fig. A-1. The average gas-side heat-transfer coefficient, as reported in Ref. A-1 is expressed as:

$$h_{g_{ave}} = 0.0145 \frac{k}{D} Pr^{1/3} \left(\frac{Re_D}{M_\infty}\right)^{0.4} \left(\frac{g_c \rho_o D^2 P_o}{\mu_o{}^2}\right)^{0.2} \left(\frac{T_o}{T_r}\right)^{0.32}, \tag{8}$$

where

$$T_r = 1/2 \, (T_{wg_o} + T_o) \tag{9}$$

In a checkout run, however, correlation between the analytical heat flux and the calorimetrically measured heat flux for uncoated tubes could only be obtained when the coefficient of equation (1) was increased from 0.0145 to 0.0247. The equation so modified was used in all subsequent calculations of $h_{g_{ave}}$ for the coated tubes.

Coating and Tube Resistance. The thermal resistance of the coating is dependent on the coating thickness and the thermal conductivity of the coating. The coating thickness was measured at four locations on one cross-section using a high-power microscope. The average of the four thickness measurements was used. The thermal conductivity of the porous zirconia coating was taken from Ref. A-3. An average steady-state coating temperature $(T_{aw} + T_{wc})/2$ was used in evaluating the thermal conductivity of the coating.

Thermal resistance of the Hastelloy-X substructure is also a function of the tube wall thickness and the thermal conductivity. The tube wall thickness was assumed constant (0.015 in), and the thermal conductivity was obtained from Ref. A-3. The average steady-state tube wall temperature $[(T_{wc} - T_{wl})/2]$ was used in selecting the thermal conductivity.

Coolant Side Heat Transfer Coefficient. The coolant-side heat-transfer coefficient was computed using a relation developed by W. S. Hines (Ref. A-4) modified by a constant, C, to account for the fact that the flow was not fully developed:

$$h_L = 0.005\ C\ \frac{k}{D}\ Re^{0.95}\ Pr^{0.4} \qquad (10)$$

The value of the constant C was taken to be 1.35, based on the recommendations given in Ref. A-5.

Calculation Procedure. The actual calculation procedure was to assume a temperature distribution (T_{wg}, T_{wc}, and T_{wl}) and calculate the local heat transfer from equation (3). The intermediate temperatures are then calculated from equations (1) and (2). The new temperature profile is used again in equation (3). Iteration continues until a specified computational accuracy is obtained.

It must be noted that the heat fluxes as a function of position around the tubes as discussed above is based upon theory, and is not an experimental result. Instead, it is an attempt to predict the experimental results using the appropriate test conditions, e.g., chamber pressure, mixture ratio, coating thickness, etc. However, some of these conditions, such as the coating thickness, its conductivity, and its roughness are neither well known nor constant around the tube. These unknown parameters can effect the magnitude of $h_g(\alpha)$.

It was shown in Ref. A-2 that the integrated average heat transfer coefficient around the circumference of the tube is equal to the heat transfer coefficient at stagnation, (when $\alpha = 0$) (see Fig. A-1). That is

$$2 \int_0^{\pi} h(\alpha)\ r\ L\ d\ \alpha = h_o\ 2\pi\ r\ L \qquad (11)$$

This average heat transfer coefficient is proportional to the average heat flux in the case of an uncoated tube, and nearly so for coated tubes. Thus, the average heat flux, which is experimentally determined by:

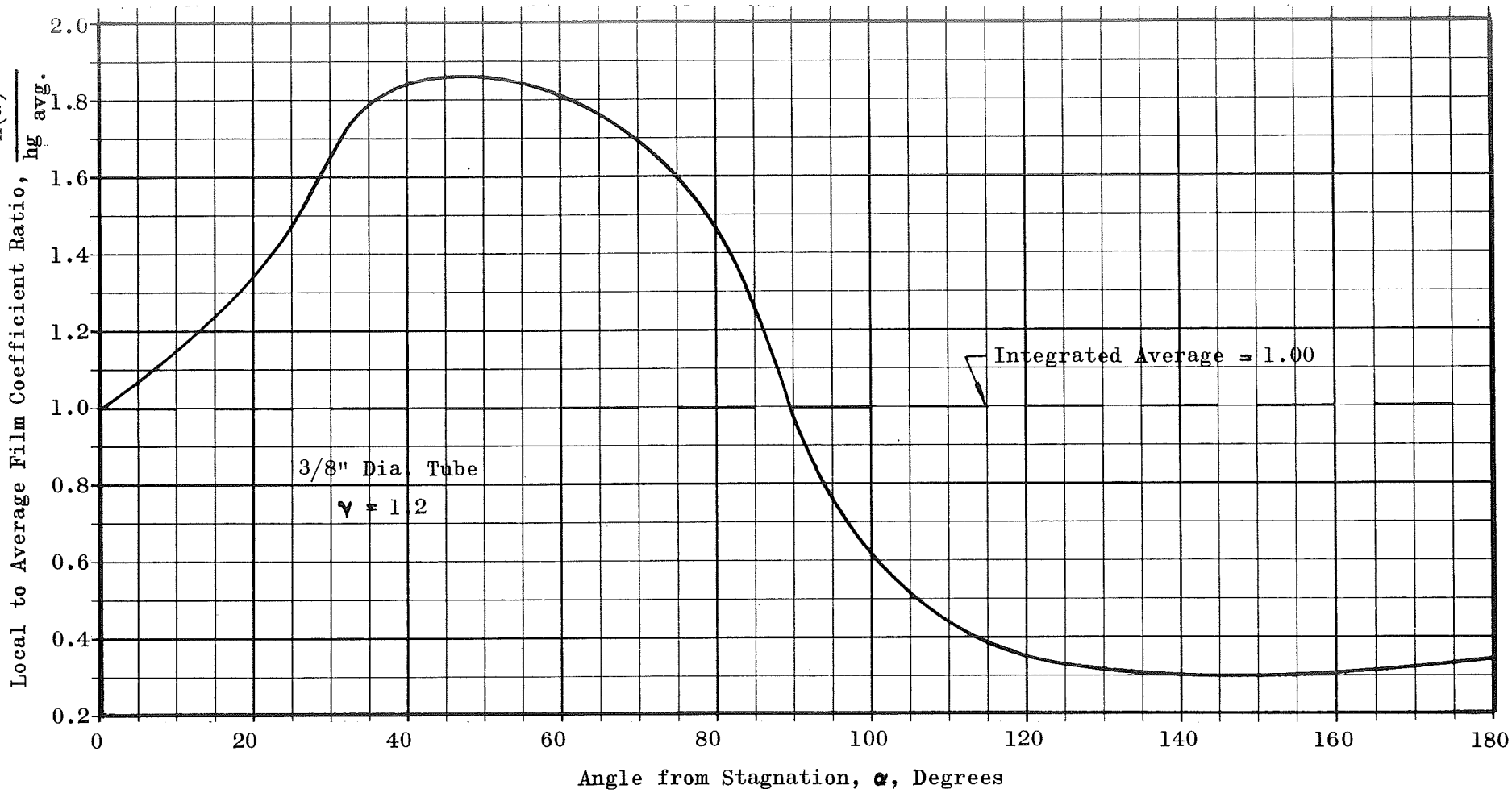

Figure A-1. Variation of Gas Side Film Coefficient with Angular Position for 3/8-inch Diameter Tube (as Reported in Reference A-1).

$$\overline{Q} = \omega c_p \quad (T_{bo} - T_{bi}) \tag{12}$$

can be compared to the theoretical heat flux at the stagnation point.

Results

The measured heat flux (average) for coated tubes varied from 12.4 to 19.1 Btu/in^2-sec. for chamber pressures over the range from about 300 to 575 psia. Although there was some scatter in the data, the results generally agree with the theory. Table A-1 shows the experimental results and theoretical predictions for these tests. In Table A-1, the actual measured heat fluxes have been corrected for incomplete combustion as discussed above. This correction is a standard correction which has been used in many rocket firing programs. It is not precisely correct in this instance, but the error is insignificant for all tests except #50.

Figures A-2 through A-4 show calculated heat flux around the tube periphery. It is seen to increase from the stagnation point to a point approximately 45 degrees from stagnation and then drop to a lower value on the downstream portion of the tube. As mentioned previously, the average heat flux is theoretically equal to that at the stagnation point.

Calculated theoretical surface temperature of the coating as a function of angular distance around the tube circumference showed, as expected, a similar relationship as compared with heat flux distribution. Figure A-5 is considered to be typical.

TABLE A-1

TASK III TEST RESULTS

Stand Run No.	Chamber Pressure (psia)	Mixture Ratio (O/F)	η_{c^*} Uncorrected %	Tube Position	Avg. Coating Thickness (Mils)	Calc'd Peak Heat Flux (Btu/in^2-sec)	Avg. Measured Heat Flux (Btu/in^2-sec)	Corrected Heat Flux $\frac{Q/A}{\eta_{c^*}}$	Calc'd Avg. (α=0) Heat Flux (Btu/in^2-sec)
50	293	6.69	94.5	(Left)	0.0	-	19.2	21.5	20.1
50	293	6.69	94.5	(Center)	1.7	-	15.0	16.7	16.0
50	293	6.69	94.5	(Right)	2.7	-	12.4	13.9	13.2
51	299	6.20	97.0	1	0.0	32.0	18.1	19.2	20.1
51	299	6.20	97.0	2	2.7	-	16.0	17.0	13.2
51	299	6.20	97.0	3	1.7	-	13.7	14.6	16.0
52	307	6.30	96.7	1	2.0	20.8	17.9	19.1	15.1
52	307	6.30	96.7	2	2.4	19.4	16.0	17.1	14.8
52	307	6.30	96.7	3	3.3	17.2	15.1	16.1	12.2
53*	449	6.12	99.0	-	0.0	36.0	-	-	22.0
53	449	6.12	99.0	1	3.1	20.1	13.3	13.6	15.6
53	449	6.12	99.0	2	1.9	22.2	17.4	17.8	18.4
53	449	6.12	99.0	3	2.5	25.0	17.8	18.2	16.8
54*	584	6.00	99.5	-	0.0	42.0	-	-	28.0
54	584	6.00	99.5	1	2.6	26.7	19.1	19.3	19.0
54	584	6.00	99.5	2	2.7	24.9	16.3	16.5	18.8
54	584	6.00	99.5	3	1.7	23.5	15.2	15.4	21.2

* Calculated values for uncoated tubes. No experimental data because of probable failure w/o coating.

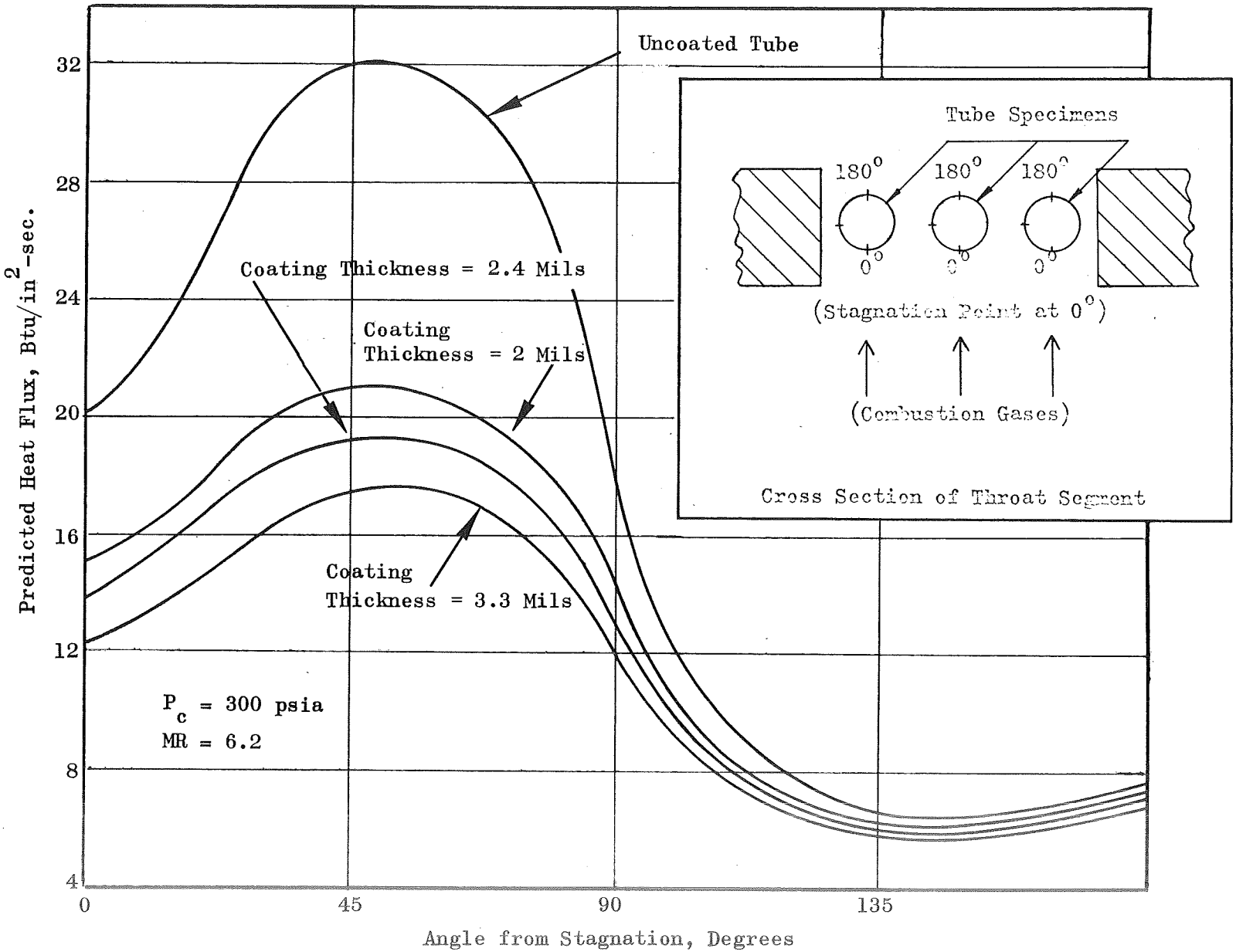

Figure A-2. Theoretical Heat-Flux Data for Coated Tubular Specimens

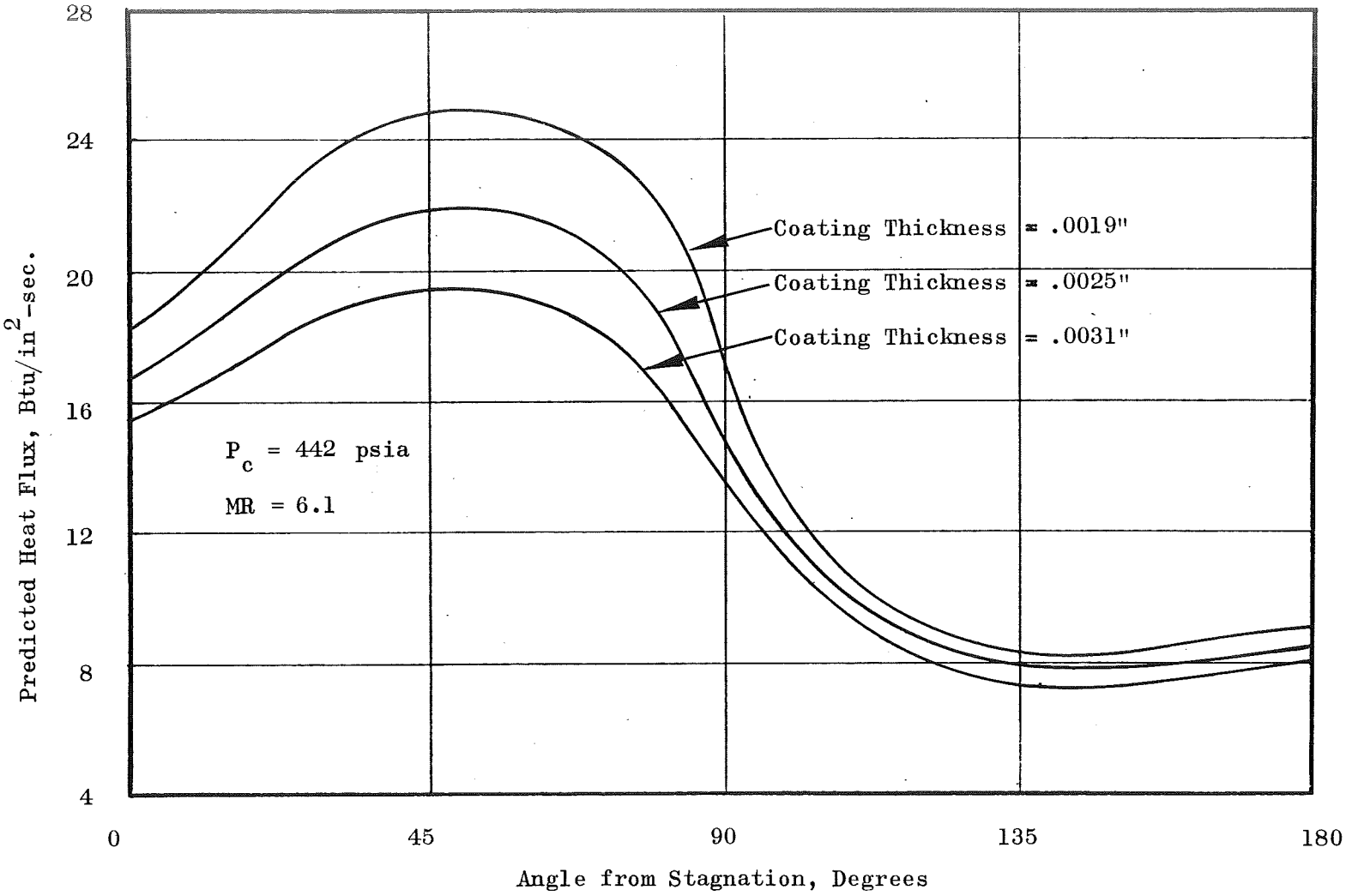

Figure A-3. Calculated Theoretical Heat-Flux Data for Coated Tubular Specimens

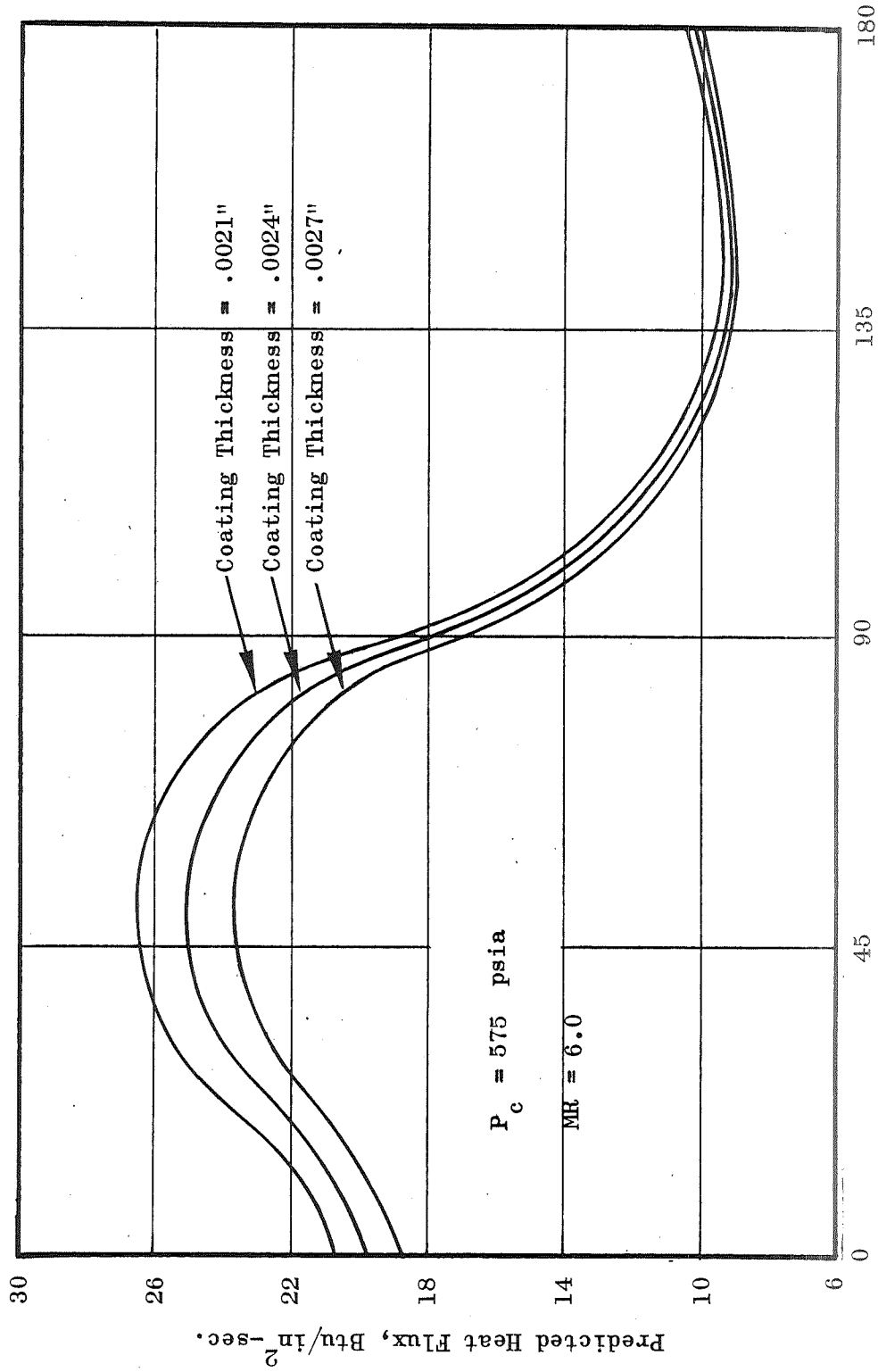

Figure A-4. Theoretical Heat-Flux Data for Coated Tubular Specimens

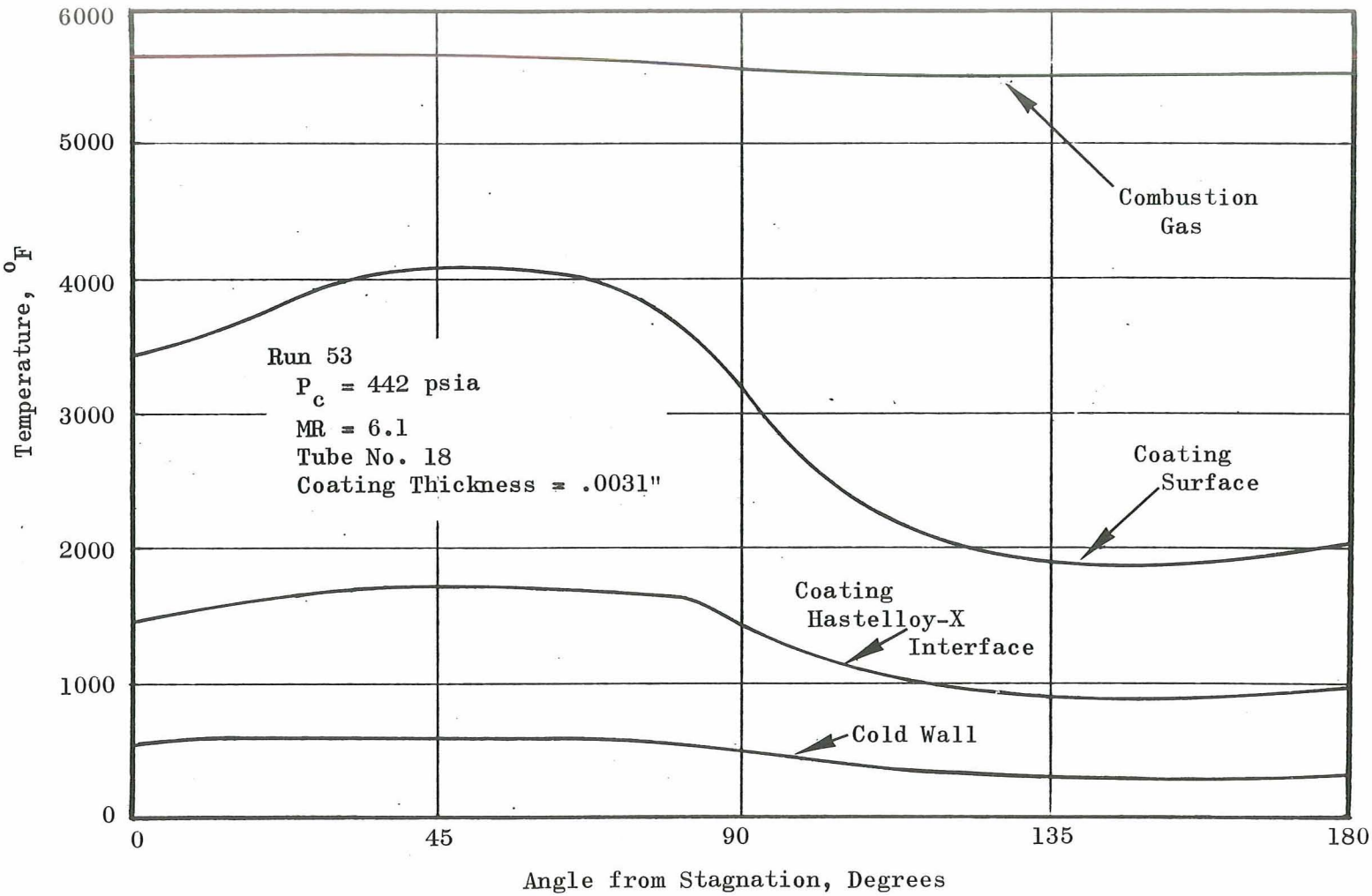

Figure A-5. Local Temperature Distribution Around the Tube Specimen

Tube position in the throat segment and slurry type had no correlatable effect on measured heat flux. Insulation capability increased somewhat with coating thickness, as expected, but there were exceptions. Nevertheless, results of these tests showed that the coating reduced heat flux 20 to 50 percent and that the coating can survive the reference rocket engine conditions.

COATED TUBULAR-WALL NOZZLE

Heat Transfer Data and Corrections

Table A-2 shows the motor operating parameters for these tests. The nozzle was two-dimensional with one of the four sides fabricated with ten 0.190 inch Hastelloy-X tubes coated with the phosphate-bonded zirconia protective coating (Fig. 4 in text). The other three sides were uncoated and flat. Calorimetric heat transfer data was taken in seven separate channels in the uncoated portion of the nozzle drilled perpendicular to the axis of the motor (Fig. A-6), while the coated tubes were manifolded together. The channels in the uncoated portion of the nozzle were numbered 4 through 10, and the coated channel was numbered 3. Water flow rates and temperature rise, measured by a three or four element thermopile, formed the heat transfer data (Table A-2).

The raw data was smoothed by plotting the heat pickup by the cooling water in each channel as a function of chamber pressure. This was particularly necessary in the case of channels 6 and 9 because the thermopiles used to measure water temperature rise were found to be defective after

TABLE A-2

HEAT TRANSFER DATA FOR THE COATED TUBULAR WALL AND THE UNCOATED COLD-WALL CALORIMETER SECTIONS IN THE TWO-DIMENSIONAL THROAT SEGMENT

Run No.	Channel No.	Chamber Pressure psia	Coolant[1] Water Flow (lbs/sec)	Change in Coolant Water Temperature ^{o} F	Calculated Heat Transfer Rate Btu/sec	Corrected[2] Heat Transfer Rate Btu/sec	Heat Flux[3] Btu/in^2-sec
90	3	244	8.16	4.56	37.5		9.25[4]
	4		1.01	14.2	14.3	13.8	11.3
	5		0.96	8.9	8.5	9.1	11.1
	6		0.985	2.4	2.4	7.2	9.9
	7		0.980	5.3	5.2	5.8	7.0
	8		0.955	10.4	7.5	7.5	8.2
	9		0.97	6.2	6.0	7.9	8.0
	10		0.955	5.3	5.1	6.3	5.2
						Total 57.6	Avg. 8.5
91	3	366	8.30	5.62	46.6		11.5[4]
	4		1.03	17.1	17.1	18.6	15.2
	5		1.02	13.3	13.5	12.7	15.4
	6		1.002	10.1	10.1	10.2	14.1
	7		1.00	8.2	8.2	8.2	9.9
	8		0.968	14.5	11.0	11.5	11.5
	9		0.994	10.6	10.5	10.9	11.0
	10		0.996	8.9	8.8	8.8	7.2
						Total 80.9	Avg. 12.0

TABLE A-2

(Concluded)

Run No.	Channel No.	Chamber Pressure psia	Coolant[1] Water Flow (lbs/sec)	Change in Coolant Water Temperature ^{o} F	Calculated Heat Transfer Rate Btu/sec	Corrected[2] Heat Transfer Rate Btu/sec	Heat Flux[3] Btu/in^2-sec
92	3	506	8.24	6.9	56.5		13.9[4]
	4		1.03	22.2	22.9	23.7	19.4
	5		0.975	17.0	16.5	16.2	19.5
	6		1.00	12.7	12.7	12.7	17.5
	7		0.998	10.4	10.4	10.4	12.5
	8		0.962	18.6	13.9	13.5	14.8
	9		0.986	14.8	14.6	14.2	14.3
	10		0.970	12.2	11.8	11.5	9.4
						Total 102.2	Avg. 15.2

(1) Water tank pressure 1350 psia.

(2) Some of these data were forced to fit a heat flux vs chamber pressure curve with 0.8 slope.

(3) Area values are listed in Table A-4.

(4) These data are uncorrected (see Table A-3 for corrected values).

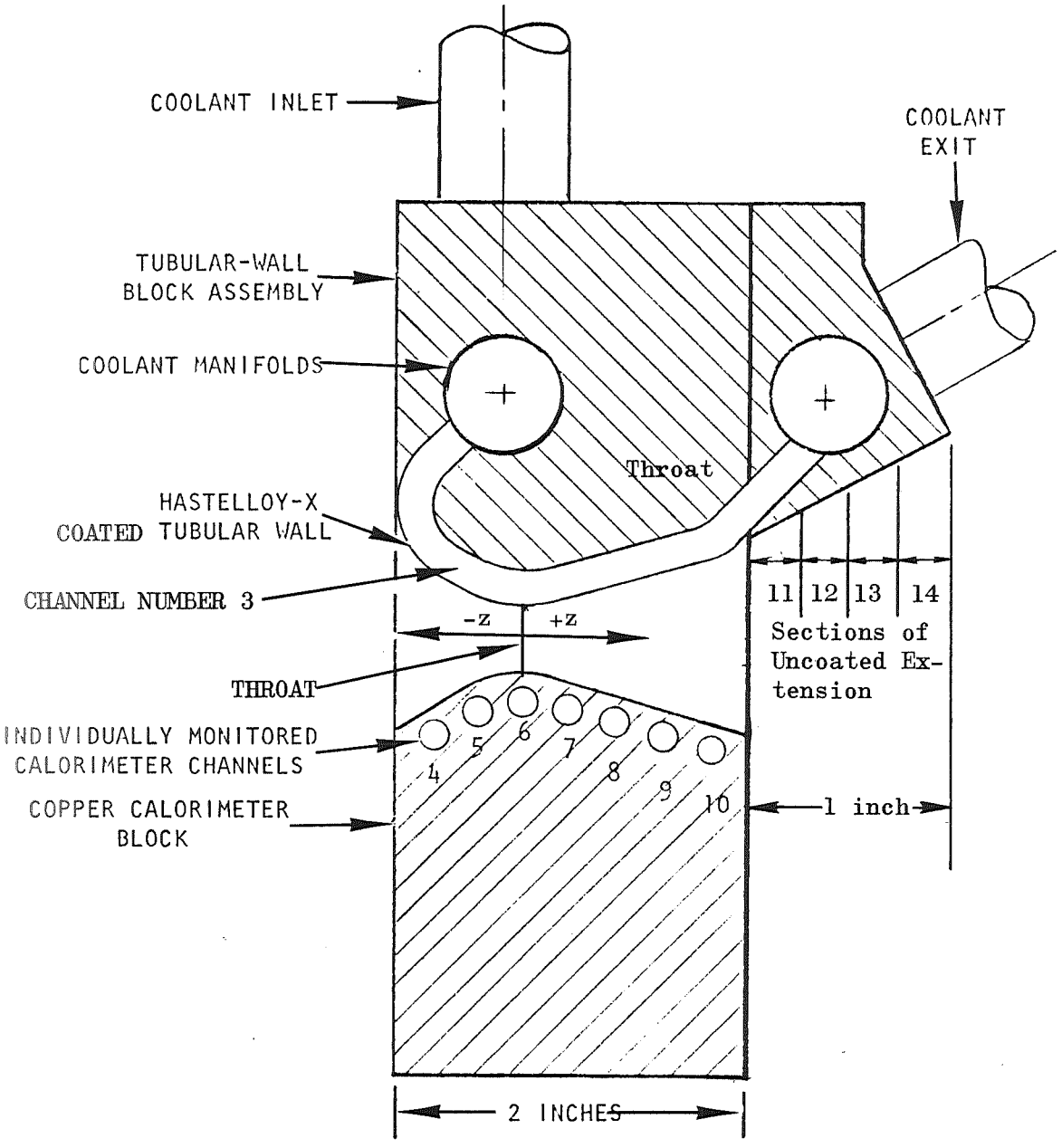

Figure A-6. Cross Section of the Two-Dimensional Throat Segment, 1.9" Wide
(See Also Fig. 6 in Text)

test #90. They were subsequently replaced. The data from channels 4 through 10 were found to lie close to straight lines with a slope of 0.8 which corresponds to the theory of turbulent boundary layer heat transfer. Utilizing this slope, all of the heat transfer data from these channels were smoothed to fit this correlation. This data smoothing process made only trivial changes in heat fluxes in test #91 and #92, but moderate increases were made in test #90 in channels 5, 7, and 10. These effects are shown in Fig. A-7. Actual data points are indicated by numbers corresponding to the channel number. Channel 9 is not shown since it is nearly co incident with number 8.

The last column in Table A-2 lists the heat flux to each channel. This is simply the heat pickup per channel divided by the area assigned to each channel. There may be some question as to the manner in which the area of the uncoated wall was divided into the seven portions, but generally, any error in apportionment of the total area is small. Table A-3 shows values used for surface area of these channels. In the case of the coated portion, however, two factors must be examined in more detail. For the moment, however, it should be noted that the value of heat flux given in Table A-2 for the coated portion is based upon only the projected area of the coated portion, and it ignores the heat transfer to the "extension" and the increase in area due to the tubular shape of the wall.

Nozzle Extension Effect. Except for the coated side, the nozzle ended at a position two inches from beginning of convergence. On the coated side, however, an uncoated copper extension continued on for another inch (Fig.

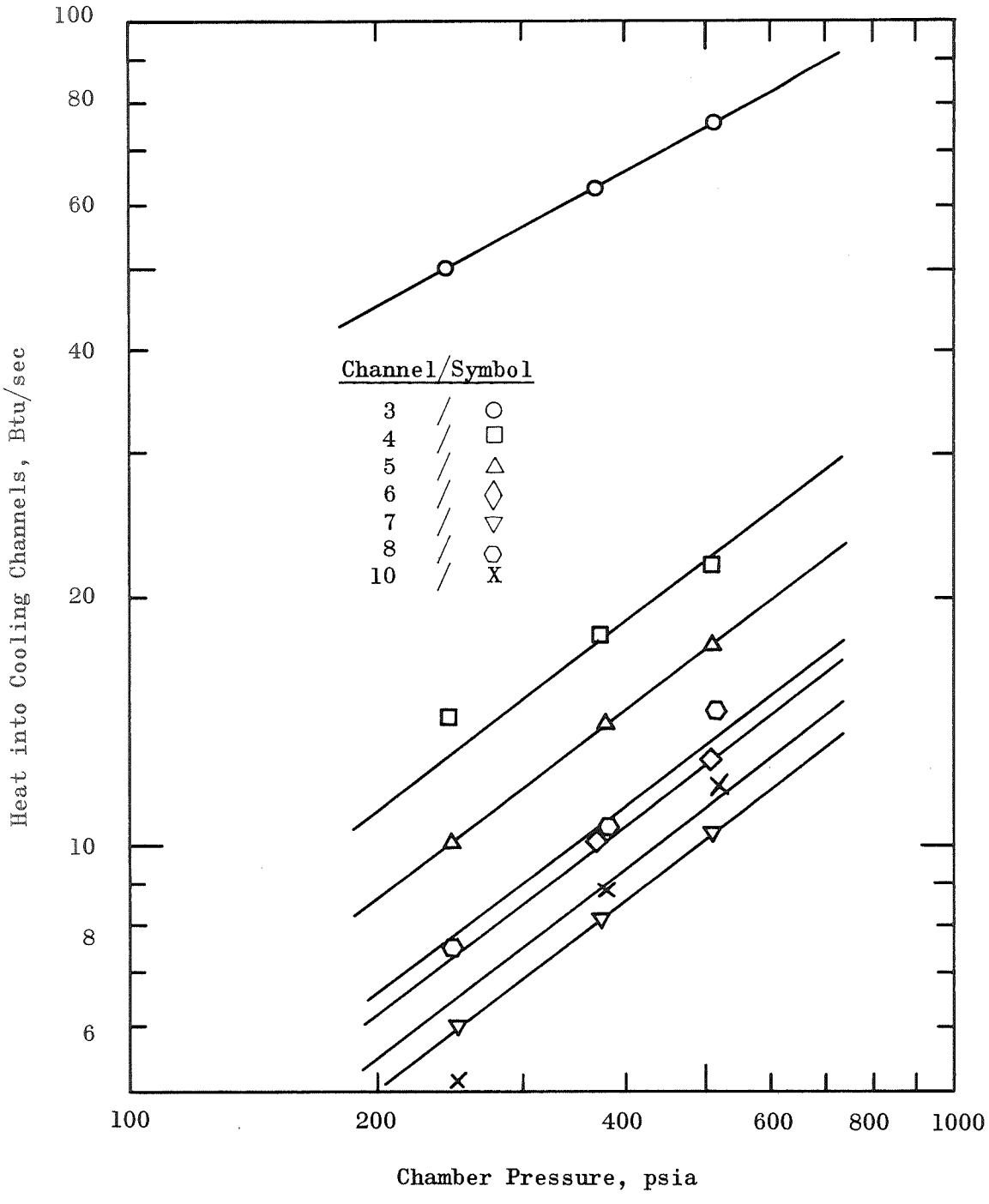

Figure A-7. Measured Heat into Coolant Channels

TABLE A-3

SURFACE AREA ASSOCIATED WITH EACH CHANNEL
IN THE TWO-DIMENSIONAL THROAT SEGMENT

Location		Surface Area (1)	A_{cs}
Channel	4	1.26	1.53
	5	0.721	1.00
	6	0.728	0.76
	7	0.826	0.78
	8	0.910	1.17
	9	0.994	1.45
	10	1.22	1.76
	Total	6.73	
Coated Wall	3	4.08 (2)	
Extension	11	0.49	2.04
	12	0.49	2.28
	13	0.49	2.54
	14	0.49	2.78

(1) Channels 4 through 10 include area of nozzle side wall

(2) Projected area, i.e., not considering the tubular contour.

A-6). This uncoated area, which was in direct contact with the exhaust gases received heat from these gases. To obtain the heat passing through the coated portion of the nozzle, this "additional" heat needs to be subtracted from the heat measured in channel number 3. The calculation of this "additional" heat is made in a simple, conservative way as discussed below and illustrated by Table A-4.

Since this calculation is expected to result in only a small correction in the heat flux to the coated nozzle, only a simple, first order, correction is made. The assumption is made that the heat flux is proportional to the mass flux through the nozzle (as shown experimentally in Fig. A-7). It is assumed that the temperature difference between exhaust gas and nozzle wall is constant (Mach number effects upon adiabatic wall temperatures are neglected), and thus the heat flux is proportional to the heat transfer coefficient at any point along the nozzle. It is further assumed that density gradient effects along the nozzle are negligible and that the effect of nozzle hydraulic radius may be ignored. With these assumptions (which are either conservative or compensating), a simple relationship may be written:

$$Q/A(z)/(Q/A)_t = \frac{h(z)}{h_t} = \left[A_t/A_{cs}(z)\right]^{0.8} \qquad (13)$$

Now it is necessary to know the area ratio as a function of nozzle length. The cross sectional area at various axial positions corresponding to the heat transfer channels was calculated and shown in Table A-3. The nozzle extension was divided into four fictitious channels: 11, 12, 13, and 14, each taken to be 1/4-inch long as shown in Fig. A-6. The surface area assigned to these channels was simply their slant length times 1.9 inches, the nozzle width. The cross-sectional area assigned at these points is the same as if the other three sides of a symmetric nozzle were present.

TABLE A-4

HEAT TRANSFER TO UNCOATED

NOZZLE CALCULATIONS

Location Channel	Distance From Throat (Inches)	$\frac{A_{cs}(z)}{A_t}$	$\left(\frac{A_{(z)}}{A(t)}\right)^{0.8}$	$\frac{h(z)}{(h_t)}$	$\frac{h(z)\ A_w(z)}{h_t}$
4	-0.549	2.02	1.75	0.572	0.7
5	-0.252	1.31	1.24	0.806	0.582
6	0	1.00	1.00	1.00	0.728
7	2.75	1.03	1.02	0.980	0.726
8	0.555	1.54	1.41	0.71	0.64
9	0.835	1.90	1.64	0.61	0.61
10	1.135	2.32	1.96	0.51	0.62
				Total	4.606
11	1.420	2.66	2.18	0.46	0.216
12	1.670	3.00	2.41	0.41	0.19
13	1.920	3.34	2.62	0.38	0.175
14	2.120	3.68	2.82	0.35	0.165
				Total	0.746

Using Eq. (13), the heat transferred into the uncoated extension can be found as a ratio of that transferred into the uncoated portion of the nozzle, channels 4 through 10 (see Table A-4).

$$Q_{11\text{-}14} = Q_{4\text{-}10} \times \frac{\sum_{11}^{14} \frac{A_w(z)\, h(z)}{h_t}}{\sum_{4}^{10} \frac{A_w(z)\, h(z)}{h_t}} = \frac{0.746}{4.606} = 0.16 \qquad (14)$$

Thus, experimentally measured heat input to channel 3 should have 16% of that from channels 4 through 10 subtracted to account for the uncoated extension, or

$$28.3 = 37.5 - 0.16 \times 57.6 \text{ for run 90}$$
$$33.6 = 46.6 - 0.16 \times 80.9 \text{ for run 91}$$
$$39.7 = 56.5 - 0.16 \times 102.2 \text{ for run 92}$$

These data are given in the second row of Table A-5.

Area Corrections. Heat transfer data results of the coated tube wall had to be adjusted for the tubular contour as opposed to a flat one, and for the variance of the boundary layer heat transfer properties in the narrow tube valleys. If the tubular coated wall were ideal, one may expect an area increase to be 57%, corresponding to $\pi/2$ as opposed to unity. Actually, of course, the increased area is not nearly that large, nor is the

TABLE A-5

CORRECTED HEAT FLUX THROUGH THE COATED WALL
COMPARED TO HEAT FLUX THROUGH THE UNCOATED CALORIMETER

Run	90	91	92
Average Heat Flux Through the Uncoated Cold-Wall Calorimeter (Btu/in^2-sec)	8.5	12.0	15.2
Heat Flux Through the Coated Tubular Wall Corrected for the Uncoated Extension (Btu/in^2-sec)	6.9	8.3	9.8
Reduction in Heat Flux	19%	30%	35%
Heat Flux Through the Coated Tubular Wall Corrected for Area (i.e., The Surface Contour) (Btu/in^2-sec)	5.9	7.1	8.4
Reduction in Heat Flux	30%	40%	46%

heat transfer in that very narrow space between tube crowns as high as that on the crown. Various geometrical calculations were devised to correct for this area effect, but the most meaningful correction, however, was found to be based on some empirical data generated at Rocketdyne some years ago for a tube wall chamber. In these tests, which also used hydrogen/oxygen as propellants and tubes of 0.090 to 0.200 inch diameter, correlations showed that an area increase of 15% best fit the data over this range. It must be realized that no direct comparison between a plane wall and a tubular wall was made, but based upon gas- and liquid-side correlations, the 15% correction factor was reasonable.

Thus, the heat flux data shown in Table A-2 were corrected using a 15% increase in projected area of the coated wall. With these corrections, which are believed to be conservative, the coating is shown to decrease the heat flux by 30, 40, and 46 percent at chamber pressures of 244, 366, and 506 psia, respectively.

Summary

If no data corrections are made, the heat flux is greater through the coated wall than through the uncoated wall at the low (244 psia) pressure. Even so, because the slopes of heat flux vs chamber pressure is so much less for the coated portion, the coated surface shows reduced heat flux at higher chamber pressures. This is shown best in Fig. A-7 where all uncoated channels show a slope of 0.8 as compared to a slope of about 0.55 for the coated channel. Thus, although the corrections for nozzle extensions and tubular area have been made (shown in Table A-5), even

the raw uncorrected data shows that a significant heat flux reduction is made with the coated surface. Figure A-8 also shows how the coating acts to reduce the heat flux by greater percentages as the absolute heat flux increases.

The exact amount of heat flux reduction for a particular thickness under a particular application environment may be somewhat indefinite, but for all but the most minimal of heat fluxes, even a small reduction in heat flux results in significant decreases in wall temperature, and, in turn, reductions in wall temperature result in lower applied stresses, higher strength, and greatly increased fatigue or creep life of the metal component.

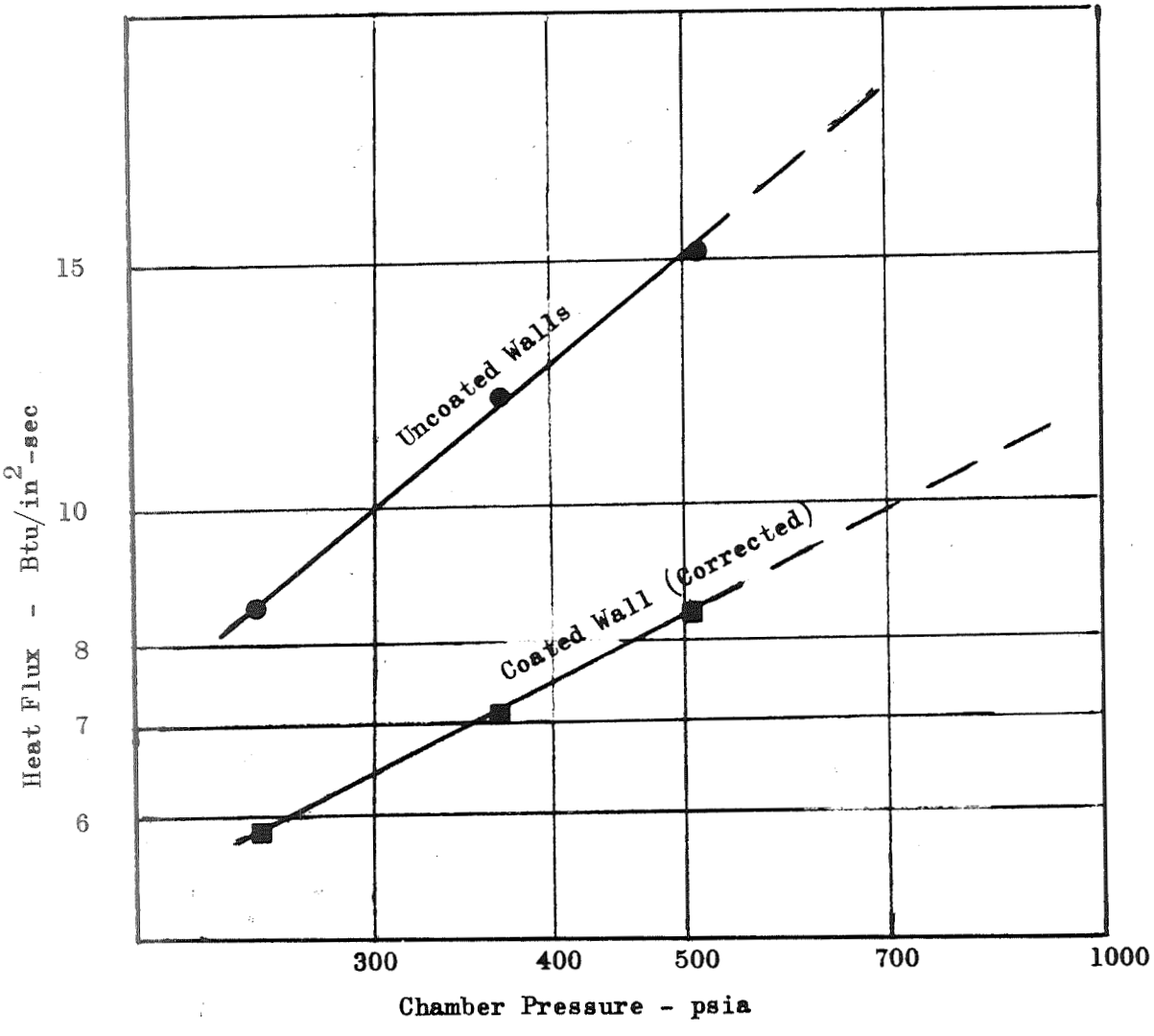

Figure A-8. Heat Flux Reduction Due to Coating

NOMENCLATURE FOR APPENDIX A

A	=	area
D	=	tube diameter
g_c	=	gravitational constant
h	=	heat transfer coefficient
k	=	thermal conductivity
L	=	exposed tube length, thickness
M	=	Mach number
Nu_D	=	Nusselt number based on diameter
P	=	pressure
Pr	=	Prandtl number
Q	=	heat input
R	=	thermal resistance
R_T	=	recovery factor
Re_D	=	Reynolds number based on diameter
r	=	radius
T	=	temperature
w	=	flowrate
z	=	axial distance from throat

Subscripts

ave	=	average
aw	=	adiabatic wall
b	=	bulk temperature
bi	=	bulk temperature in
bo	=	bulk temperature out

c	=	coating
cs	=	cross sectional
g	=	gas side
H	=	Hastelloy
l	=	liquid
o	=	stagnation
r	=	reference temperature
sat	=	saturation
t	=	throat
theo	=	theoretical
w	=	wall
wc	=	coating/tube interface
∞	=	free stream
1	=	tube ID
2	=	coating/tube interface
3	=	gas side

Greek

γ	=	gas specific heat ratio
ρ	=	density
μ	=	viscosity
η_{c^*}	=	uncorrected characteristic velocity efficiency
α	=	angle from stagnation point

APPENDIX A - REFERENCES

A-1. Talmor, E., "Heat Transfer to Small Diameter Throat Tubes," printed in Symposium on Selected Papers-I, 56th National Meeting of American Institute of Chemical Engineers, San Francisco, California, 16-19 May 1965.

A-2. Talmor, E., "Toroidal Tube Heat Transfer With and Without Film Cooling," Research Report 63-28, Rocketdyne, October 1963.

A-3. "Thermophysical Properties of High Temperature Solid Materials," Y. S. Youloukian, Editor, Thermophysical Properties Research Center, Purdue University, The MacMillan Company, New York, New York.

A-4. Hines, W. S., "Turbulent Forced Convection Heat Transfer to Liquids at Very High Heat Fluxes and Flowrates," RR 61-14, Rocketdyne, 30 November 1961.

A-5. McAdams, W. H., "Heat Transmission," McGraw-Hill Book Company, Inc., 1954.

A-6. Southern Research Institute, "The Thermal Properties of Twenty-six Solid Materials to 5000 F or Their Destruction Temperatures," Technical Document Report No. ASD-TDR-62-765, January 1963.

A-7. Goldsmith, A., H. J. Hirschhorn, T. E. Waterman, "Thermophysical Properties of Solid Materials," Vol. III Ceramics, AD No. 265597, November 1960.

DISTRIBUTION LIST

		No. of Copies
National Aeronautics and Space Administration Lewis Research Center 21000 Brookpark Road Cleveland, Ohio 44135		
Attention:	Contracting Officer Chemical Rocket Procurement Section Mail Stop 500-210	13
National Aeronautics and Space Administration Washington, D.C. 20546		
Attention:	Code RPL	2
	Code RPX	1
	Code RRM	1
Scientific and Technical Information Facility NASA Representative, Code CRT Post Office Box 33 College Park, Maryland 20740		6
National Aeronautics and Space Administration Langley Research Center Langley Station Hampton, Virginia 23365		
Attention:	Robert R. Howell & John D. Buckley Mail Stop 208	2
	Librarian	1
National Aeronautics and Space Administration Goddard Space Flight Center Greenbelt, Maryland 20771		
Attention:	Librarian	1
National Aeronautics and Space Administration Marshall Space Flight Center Huntsville, Alabama 35812		
Attention:	K. Chandler, R-P&VE-PA	1
	Librarian	1
	Marshall King, R-P&V-MNC	1

	No. of Copies
National Aeronautics and Space Administration Ames Research Center Moffett Field, California 94035	
Attention Librarian	1
National Aeronautics and Space Administration Manned Spacecraft Center Houston, Texas 77085	
Attention: J. G. Thibodaux & S. Jacobs	2
Librarian	1
Jet Propulsion Laboratory 4800 Oak Grove Drive Pasadena, California 91103	
Attention: Librarian	1
National Bureau of Standards U.S. Department of Commerce Washington, D.C. 20546	1
Department of the Air Force Air Force Materials Laboratory (AFSC) Wright Patterson Air Force Base, Ohio 45433	
Attention: MAMC (J. J. Krochmal)	1
Department of the Air Force Air Force Rocket Propulsion Laboratory Attention: RPM Edwards Air Force Base, California 93523	1
Department of the Army Picatinny Arsenal Scientific & Technical Information Branch Attention: SMUPA-VA6, Librarian Dover, New Jersey 07801	1
U.S. Army Materials Research Agency Watertown, Massachusetts	1
Department of the Navy Naval Research Laboratory Attention: Code 2027 Washington, D.C., 20390	1

	No. of Copies
Norton Research Corporation Attention: Technical Information Center 70 Memorial Drive Cambridge, Massachusetts 02142	
Philco Ford Corporation Aeronutronic Division Attention: Technical Information Service Acquisitions Ford Road Newport Beach, California 92663	1
Southern Research Institute Menlo Park, California	1
Stanford Research Institute Document Center for Propulsion Sciences 333 Ravenswood Avenue Menlo Park, California 94025	1
Sylvania Electric Products, Incorporated Silcor Division Hicksville, New York	1
Teleflex, Incorporated Sermetal Division P.O. Box 187 125 South Main Street North Wales, Pennsylvania 19454	1
TRW Systems, Incorporated Attention: Technical Information Center One Space Park Redondo Beach, California 90278	1
Union Carbide Corporation P.O. Box 324 Tuxedo, New York 10987	
Attention: Technical Librarian	1
United Aircraft Corporation Attention: Acquisitions Librarian 400 Main Street East Hartford, Connecticut 06108	1

	No. of Copies
General Motors Technical Center 12 Mile and Mound Road Warren, Michigan	
Attention: Dr. Richard Murie, Dept. 55	1
General Telephone & Electronics Laboratory, Inc. Bayside, New York	1
IIT Research Institute 10 West 35th Street Chicago, Illinois 60616	
Attention: Document Library	1
International Harvester Company Solar Division San Diego, California 92112	1
Itek Corporation Vidya Division 1450 Page Mill Road Palo Alto, California 94304	
Attention: Librarian	1
LTV Aerospace Corporation LTV Vought Aeronautics Division Attention: Librarian P.O. Box 5907 Dallas, Texas 75222	1
The Marquardt Corporation Attention: Librarian P.O. Box 2013 South Annex Van Nuys, California 91409	1
McDonnell-Douglas Corporation Douglas Missile and Space Systems Division Attention: Librarian A2-260 & Norman Harris 3000 Ocean Park Blvd. Santa Monica, California 90406	2
Monsanto Research Corporation Attention: Security Office 1515 Nicholas Road Dayton, Ohio 45407	1

	No. of Copies
Department of the Navy Naval Air Systems Cmd. Attention: AIR-330 Washington, D.C. 20360	1
DMIC Battelle Memorial Institute Columbus Laboratories 505 King Avenue Columbus, Ohio 43201	
Attention: Information Specialist	1
Defense Ceramic Information Center Battelle Memorial Institute Columbus Laboratories 505 King Avenue Columbus, Ohio 43201	
Attention: Manager of Technical Information	1
Chemical Propulsion Information Agency Applied Physics Laboratory - JHU 8621 Georgia Avenue Silver Spring, Maryland 20910	2
Rocketdyne, a division of North American Rockwell Corporation 6633 Canoga Avenue Canoga Park, California 91304	20 + Spares
Attention: W. T. Chandler D/589-198 BA26	
Aerojet-General Corporation P.O. Box 15847 Sacramento, California 95813	
Attention: W. J. Lewis, Dept. 0726	1
Aerojet-General Corporation Attention: Technical Library - 2432-2015A P.O. Box 15847 Sacramento, California 95813	1

	No. of Copies
Aerospace Corporation Attention: Technical Information Center-Document Group P.O. Box 95085 Los Angeles, California 90045	1
Battelle Memorial Institute Columbus Laboratories 505 King Avenue Columbus, Ohio 43201	
Attention: D. E. Kizer	1
Bell Aerosystems Company Attention: Technical Library P. O. Box 1 Buffalo, New York 14240	1
Bell Telephone Laboratories Mountain Avenue Murray Hill, New Jersey 07974	1
Boeing Company Attention: Aerospace Library 8k-38 P.O. Box 3999 Seattle, Washington 98124	1
Central Research Laboratory Allied Chemical Corporation P.O. Box 309 Morristown, New Jersey 07960	
Attention: E. R. Degginger	1
DuPont Company Eastern Division Attention : Report Clerk. A. R. Steward Gibbstown, New Jersey 08027	1
General Dynamics Corporation P.O. Box 12009 San Diego, California 92112	
Attention: Library & Information Services	1
General Electric Company Attention: FPD Technical Information Center Building 700, Mail Zone N-32 Cincinnati, Ohio 45215	1

	No. of Copies
United Technology Center Attention: Technical Library P.O. Box 358 Sunnyvale, California 94088	1
University of California Lawrence Radiation Laboratory Attention: Technical Information Division P.O. Box 808 Livermore, California 94550	1
University of Dayton Dayton, Ohio	1
University of Denver Denver Research Institute Attention: Security Officer P.O. Box 10127 Denver, Colorado 80210	1
University of Utah Attention: Dr. S. D. Brown Salt Lake City, Utah 84112	1
Vitro Laboratories West Orange, New Jersey	1